UNIVERSITY OF CALIFORNIA,
IRVINE

Developing Near-infrared Emitting DNA-stabilized Silver Nanoclusters for Biomedical Imaging

THESIS

submitted in partial satisfaction of the requirements
for the degree of

MASTER OF SCIENCE

in Materials Science and Engineering

by

Malak Rafik

Thesis Committee:
Assistant Professor Stacy Copp, Chair
Associate Professor Jered Haun
Associate Professor Michelle Digman

2022

DEDICATION

To

my family

for always loving, supporting, and believing in me.

TABLE OF CONTENTS

LIST OF FIGURES

Page

LIST OF TABLES

Page

ACKNOWLEDGMENTS

I would like to thank my advisor, Prof. Stacy Copp for her inspiration and encouragement to attend UCI. Not only did I learn so much from her throughout my academic studies and projects, but I also treasure the character-building life lessons she taught me that I will always carry with me. I truly appreciate the support, guidance, and opportunities she has generously provided. I would also like to thank my research colleagues for their valuable advice, support, and insightful feedback throughout my research. I would like to extend my deepest gratitude to my family and friends for their continuous and unconditional love, support, and encouragement throughout my studies. I am immensely indebted to the Office of Access and Inclusion for supporting my studies and granting me the Pathway to PhD fellowship which helped to make this achievement possible and all efforts fruitful. This work was supported by NSF Biophotonics CBET-2025790.

ABSTRACT OF THE THESIS

Developing Near-infrared Emitting DNA-stabilized Silver Nanoclusters for Biomedical Imaging

by

Malak Rafik

Master of Science in Materials Science and Engineering

University of California, Irvine, 2022

Professor Stacy Copp, Chair

Advancements in bioimaging modalities have changed the face of modern medicine. However, current techniques such as MRI and CT utilize hazardous radiation, contrast agents with toxic effects, and possess with limited resolution for deep tissue imaging on length scales relevant for cellular processes. *In vivo* fluorescence imaging in the near-infrared (NIR) window (750-1700 nm) is an emerging deep tissue imaging technique that offers the possibility of achieving micron-scale spatial resolutions for clearer images of anatomical structures in real time. This thesis develops NIR-emissive DNA-stabilized silver nanoclusters (Ag_N-DNAs) as fluorophores for non-hazardous fluorescence imaging. We focused on studying the chemical and photophysical properties of Ag_N-DNAs emitting in NIR I (650-950 nm) wavelengths. First, we worked towards tuning the synthesis conditions to optimize the chemical yields of these nanoclusters, purifying monodisperse and single-emissive species in solution, and determining their chemical compositions. Additionally, we tested the stability of NIR-emissive Ag_N-DNAs in physiological conditions and aimed to protect these nanoclusters against degradation to evaluate their applicability for fluorescence imaging**.** We found that the post-reduction temperature used for the nanoclusters after synthesis can significantly increase the brightness of known NIR-emissive Ag_N-

DNAs and decrease the time it takes to achieve maximum emission intensity. Also, new Ag_N-DNAs were found to evolve from red emissive Ag_N-DNAs upon changing post-reduction conditions. Mass-spectra of HPLC-purified NIR-emissive Ag_N-DNAs indicate that these nanoclusters are stabilized by 2 DNA strands, containing six neutral silver atoms and, in some cases, chloride ligands. Attempts to use polyamines to stabilize the Ag_N-DNAs in saline conditions did not aid in protecting them from emission quenching, but instead, some nanoclusters were found to be stable on their own without modification. Lastly, preliminary *in vivo* experiments utilized a promising NIR-emissive Ag_N-DNA in a mouse model, which displayed bright luminescence for several hours while indicating no overt signs of toxicity to the mouse's liver or spleen. This work laid the groundwork for improved fundamental understanding of methods to discover new NIR-emissive Ag_N-DNAs, optimize their chemical yields, and establish them as suitable and safe fluorophores for bioimaging techniques.

INTRODUCTION

Advancements in biomedical imaging techniques have been critical for the progress of fundamental biomedical science and clinical practice. Current biomedical imaging techniques that are heavily used for clinical applications include computed tomography (CT), magnetic resonance imaging (MRI), positron emission tomography (PET), single-photon emission computed tomography (SPECT), and ultrasound scanners. These imaging modalities have all changed the face of medicine, from disease diagnosis and monitoring to surgical techniques. However, these techniques often utilize hazardous radiation and/or toxic contrast agents to resolve tissue structure, and their resolutions are typically limited to millimeter scales. In contrast, optical microscopy uses non-hazardous electromagnetic radiation and can achieve micron-scale spatial resolutions *in vivo*.

Fluorescence microscopy, a promising type of optical microscopy, uses fluorophores to provide contrast to tissues and other targets of interest and can be used to acquire images in real time.[1] Since biological tissue can absorb and emit photons of visible light (400-750 nm),[9] fluorescence microscopy uses the separation of excitation and emission spectra to capture images. There is a special interest in fluorescence microscopy using near-infrared (NIR) wavelengths in comparison to visible light fluorophores. Visible light can only penetrate 10 - 100 μm within biological tissue due to the high scattering coefficients, autofluorescence, and strong absorbance of hemoproteins and other constituents of biological tissues and fluids *(Fig. 1B, C).* Alternatively, NIR light can penetrate several centimeters into tissues, making NIR fluorescence imaging a promising deep tissue imaging technique that can visualize very specific biological moieties like cellular mapping, [10] single motor proteins traversing microtubules,[11] and target biolabels. This technique offers the possibility of resolving clearer images of anatomical structures and even specific imaging of biomolecules and molecular-scale physiological functions.[1]

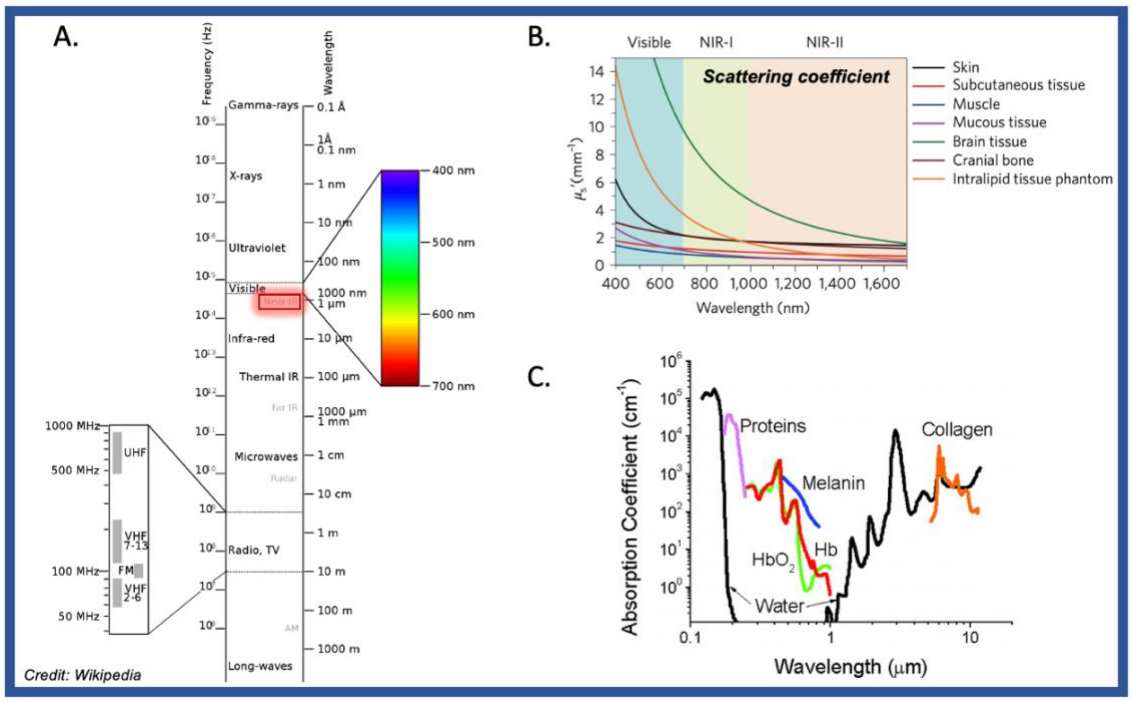

Figure 1. *A) The electromagnetic spectrum, with annotations identifying the wavelengths for visible and NIR light. B) Reduced scattering coefficient of light by different physiological structures from visible to NIR II window.*[1] *C) Absorption coefficient of physiological tissue and blood components from 200 nm to 10 µm.*[2]

At present, NIR deep tissue bioimaging is limited by a lack of bright, biocompatible light-emitting biolabels that can provide contrast to tissues and other targets. NIR fluorophores include fluorescent organic dye molecules and fluorescent proteins, as well as NIR-emitting nanoparticles such as semiconductor quantum dots and carbon nanotubes. Organic molecules are heavily used for fluorescence microscopy since these molecules come in a diverse range of excitation and emission wavelengths *(Fig. 2)*. These organic dyes can be costly to synthesize and conjugate to biomolecules, and their fluorescence brightness diminishes significantly at NIR wavelengths. NIR organic dyes and fluorescent proteins suffer from low quantum yields and/or extinction

coefficients. Bright NIR-emitting nanoparticles often suffer from unfavorable toxicities and have large sizes compared to nanometer-sized biomolecules.

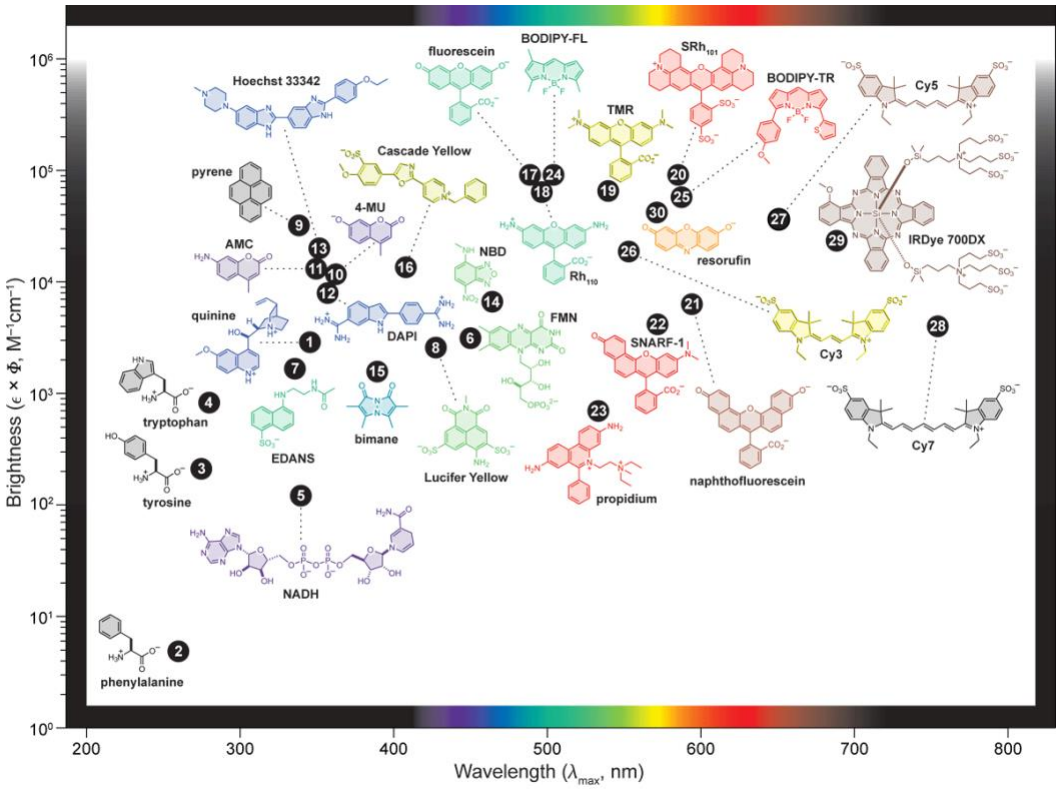

Figure 2. *Examples of organic molecule fluorophores showing their absorbance wavelengths and brightness.* [3]

Metal nanoclusters are a new promising class of NIR fluorophores that could enable deep tissue bioimaging with fluorescence microscopy. Nanoclusters are the smallest of nanoparticles, containing just 2 – 10^2 metal atoms. At such tiny sizes, these nanomaterials begin to exhibit molecular-like and luminescence properties. For example, Au, Ag, and Cu nanoclusters with metal cores > 2 nm in size can exhibit bright luminescence, enhanced catalytic activity, and low toxicity levels compared to larger nanoparticles (5-100 nm). At this size regime, nanocluster properties are highly sensitive to their composition and shape, which can be used to precisely tune photophysical properties and photostability. Researchers use protecting ligands such as thiolates, phosphines, or metal-coordinating biomolecules to stabilize these nanoclusters in solution. DNA- and protein-

templated nanoclusters are especially promising for bioimaging, due to their increased water solubility and biocompatibility.[4] This inspires a wide range of biological applications, from tissue imaging to biosensing, diagnosis, and biomedical therapy *(Fig. 3).*[4]

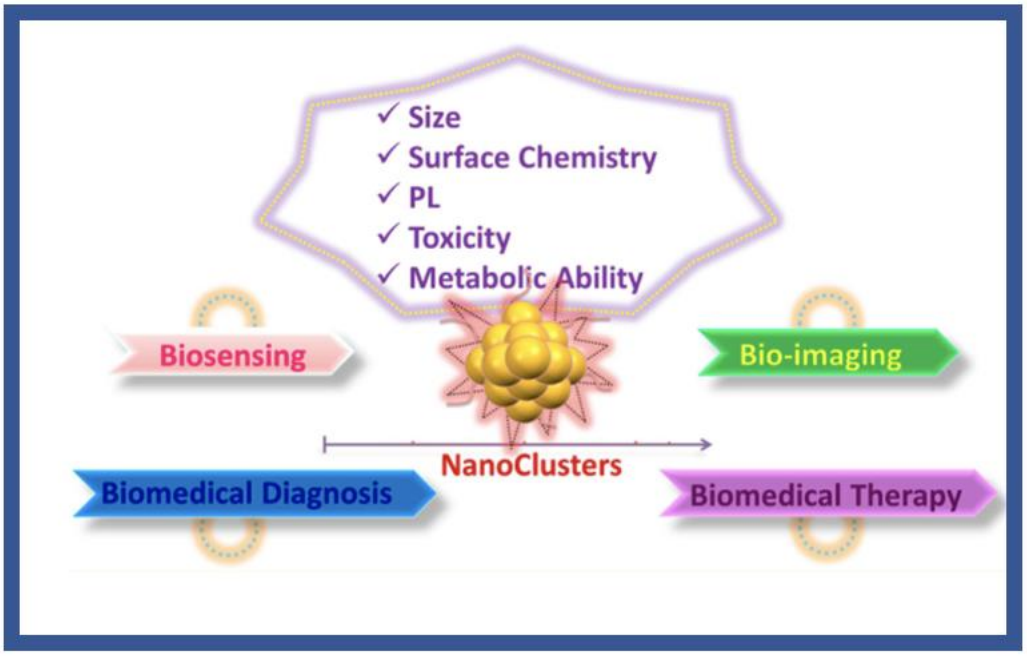

Figure 3. *Biomedical applications of nanoclusters and their promising properties.*[4]

DNA-stabilized silver nanoclusters (Ag_N-DNAs) are a unique class of programmable nanocluster fluorophores with unusually high promise for NIR bioimaging applications. Ag_N-DNAs are stabilized by single-stranded DNA oligomers that encapsulate just 10-30 silver atoms *(Fig. 4A).* Due to their tiny sizes and highly anisotropic rod-like shapes, Ag_N-DNAs exhibit bright nanosecond-lived fluorescence *(Fig. 4B).* Moreover, Ag_N-DNAs combine this favorable bright fluorescence with the unique sequence-encoding property of DNA template. Because DNA has sequence-dependent interactions with silver cations,[12] the DNA sequence selects the size and shape of the silver nanocluster. Tuning the DNA template sequence has enabled researchers to stabilize

a wide range of Ag_N-DNAs with emission wavelengths from 450 nm (visible blue light) up to 1,200 nm (NIR).[13]

The fluorescence excitation and emission spectra of Ag_N-DNAs are strongly correlated to the nanocluster's size and shape. Ag_N-DNAs are partially reduced, meaning that the total number of silver atoms N is greater than the number of effective neutral silver atoms, N_0. Since silver has an electron configuration of $4d^{10}\ 5s^1$, each neutral silver atom contributes one valence electron to the nanocluster, forming metallic bonds between Ag atoms. Like other ligand-stabilized metal nanoclusters, N_0 strongly affects the optical properties of the nanocluster.[14] The strong correlation of peak fluorescence wavelength with N_0 for Ag_N-DNAs led to the discovery that fluorescent Ag_N-DNAs have rod-like shapes. Effective valence electron counts of N_0= 4, 6, 10 and 12 neutral Ag atoms are the 'magic numbers' for Ag_N-DNAs, unlike the magic numbers 2, 8, 18, … of spherical metal nanoclusters. Studies have shown that green-emissive Ag_N-DNAs have N_0 = 4, red-emissive Ag_N-DNAs have N_0= 6, and the few known NIR-emissive Ag_N-DNAs have N_0 = 10-12. Recent studies find that some Ag_N-DNAs also have spherical shapes and N_0 = 8.[8] Only one purified Ag_N-DNA (name GG322 which refers to its specific DNA template strand) that emits at 737 nm, has a resolved structure *(Fig. 4C).* All Ag_N-DNAs can also be "universally" excited through the UV excitation of the DNA strands, in addition to the size/shape dependent visible or infrared peak of each Ag_N-DNA, and this useful property allows high-throughput experimental screening of 10^3 Ag_N-DNAs with a single excitation wavelength *(Fig. 4D*).[8]

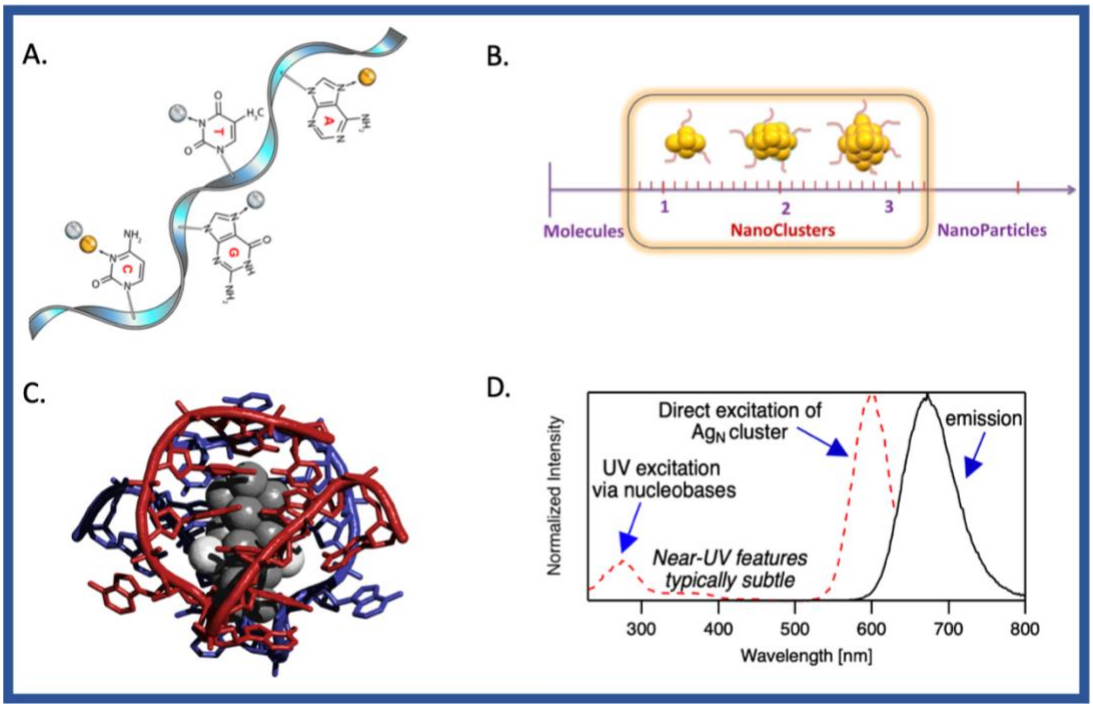

Figure 4. *A) A single-stranded DNA with the four nucleobases showing their primary metal-coordination location for gold and silver atoms;*[5] *B) nanocluster size compared to molecules and nanoparticles;*[4] *C) the resolved X-ray crystal structure of GG322*[6] *and D) an example of excitation and emission spectra of Ag$_N$-DNAs.*[7]

Hundreds of DNA sequences have been identified that create Ag$_N$-DNAs with emission wavelengths in the visible range, and a growing number of Ag$_N$-DNAs have been identified in the lower NIR I (650-950 nm) window. However, almost no Ag$_N$-DNAs have been identified that emit in the NIR II (1000-1350 nm) window. Ag$_N$-DNA fluorescence wavelengths are heavily influenced by the nucleobase sequence of the templating DNA strand, which selects the number of silvers cations and neutral silvers in the nanocluster. Because this sequence-to-color relationship is complex, researchers are employing machine learning in conjunction with high throughput experiments to design NIR Ag$_N$-DNAs. These approaches have recently uncovered several dozen new NIR Ag$_N$-DNAs,[13] but the chemical properties of these nanoclusters are not well understood.

In order to determine the composition of an Ag$_N$-DNA species and relate this composition to its chemical and optical properties, it is necessary to study compositionally pure solutions of Ag$_N$-

DNAs. Purification ensures that a sample of Ag_N-DNAs will contain only one type of nanocluster with the same number of silver atoms and the same luminescence properties. Ag_N-DNA synthesis involves mixing DNA strands and silver nitrate in aqueous solution for fifteen minutes, followed by reducing the mixture with sodium borohydride. Like most chemical synthesis processes, Ag_N-DNA synthesis produces a range of different silver-DNA products, not just a single fluorescent nanocluster species. High performance liquid chromatography (HPLC) can then be used to isolate a single species of Ag_N-DNA emitter from the rest of the products formed by chemical reduction, including DNA-silver complexes and larger silver nanoparticles. An Ag_N-DNA's spectra are compared before and after purification to ensure that purification does not alter or degrade the nanocluster.

To develop NIR-emissive Ag_N-DNAs for *in vivo* optical microscopy bioimaging, this thesis reports the chemical and optical properties of NIR Ag_N-DNAs as well as strategies for increasing the chemical yield of their synthesis and increasing their stability in physiological conditions. Because nanocluster synthesis is performed in aqueous solution that differs from physiological ionic strength conditions, it is important to determine if Ag_N-DNAs can maintain their properties in biologically salt conditions. My thesis focuses on four different aspects of this issue: optimizing NIR-emissive Ag_N-DNA nanocluster's synthesis chemical yield, purifying, and characterizing these nanoclusters, stabilizing Ag_N-DNAs against degradation in sodium chloride (NaCl) and phosphate buffered saline (PBS), and testing these fluorophores *in vivo*.

CHAPTER 1: Experimental methods for Ag_N-DNA synthesis and optimization

Part 1

Ag_N-DNA synthesis: DNA oligomers were ordered from Integrated DNA Technologies with standard desalting and were hydrated to the desired concentration and stored at –20 °C until use. Specific DNA oligomers with 10 base sequences were chosen using a combination of high throughput experiments and machine learning models.[13] All Ag_N-DNAs were synthesized by mixing H_2O and NH_4OAc at pH 7, followed by the addition of $AgNO_3$ in a microcentrifuge tube *(Fig. 1.1).* The sample was then incubated at room temperature for 15 minutes. A freshly prepared aqueous solution of $NaBH_4$ was added to the Ag^+-DNA mixture, reducing the solution to form nanoclusters. It is important to note that $NaBH_4$ should be added at 15 minutes and that variations in incubation can affect product yield. Each solvent addition was followed by mixing by vortexing and using a mini centrifuge for a few seconds. Ag_N-DNAs were then stored at 4 °C in the dark. To determine the conditions that lead to the highest yield for each Ag_N-DNA, stoichiometry sweeps to vary [Ag^+]:[DNA] ratios and post-reduction temperature experiments were employed. In part 2 of this chapter, we will explain the experimental details of the stoichiometry sweeps of silver cations and DNA to improve the chemical yield. In part 3, we will discuss the experimental methods used to optimize the post-reduction temperature of AgN-DNAs after synthesis.

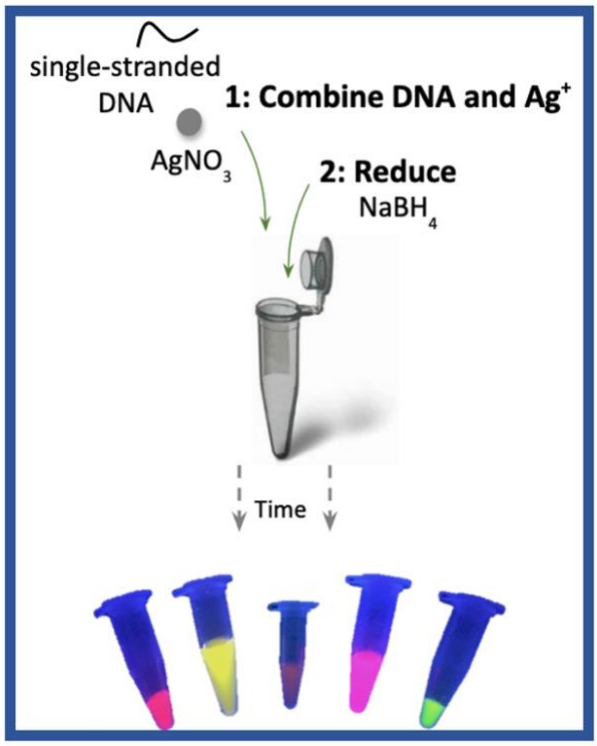

Figure 1.1. *Schematic showing the steps for Ag_N-DNA synthesis.*[7]

Materials:

Table 1.1. *Final concentrations determined to optimize the chemical synthesize of Ag_N-DNAs used throughout the thesis.*

Ag_N-DNA name	**DNA Sequence (5'-3')**	**NH_4OAc [mM]**	**DNA [µM]**	**$AgNO_3$ [µM]**	**$NaBH_4$ [µM]**
Greengen268	CCCGGAGAAG	10	20	100	50
Greenmarkov19	AGTCACGACA	10	30	150	75
Greengen332	GCAAGAGCTT	10	25	187.5	93.75
Greenmarkov18	ATCTCCACAG	10	25	100	50
Petty900	CCCACCCACC CACCCG	10	25	375	187.5
10basegen354	CGAACCGGGC	10	25	187.5	93.75
10base00419	ACCTGGACCG	10	25	197.5	93.75

Greenmarkov119	AATAACCCAC	10	25	187.5	93.75
Greentrans77	GGACAAAGAC	10	25	187.5	93.75
10base00222	TCGTTCAAGG	10	25	187.5	93.75
Greengen313	CCAAGAATAG	10	25	187.5	93.75
10base00572	ATTCTTCTTG	10	25	187.5	93.75
Allten699153	GGGGGTACAA	10	20	150	75
Allten50453	AATACCACCA	10	20	150	75
10basegen151	ATCCCACCTC	10	20	150	75
Allten698369	GGGGGAAAAA	10	25	187.5	93.75
Allten698433	GGGGGACAAA	10	25	187.5	93.75
Greentrans40	GATCTAGACC	10	20	200	100
10basegen443	GACGACGGAT	10	35	175	87.5
10basegen59	ACCCGGCGCG	10	20	200	100
10basegen203	CACCCCGAGC	10	20	300	150
Greengen159	TGCGAGAAGG	10	10	50	25
10basegen336	CCGTCCCGCC	10	20	100	50
Veryredmotif42	GTGGGGTCCG	10	20	100	50
Veryredmotifmarkov95	CCGGGGGACC	10	20	100	50
Allten349536	CCCCCCCCTT	10	25	125	62.5
10basegen66	ACCGCCGGGA	10	25	300	150
10basegen595	GGGCAGGAGA	10	25	187.5	93.75

10base00384	GGGGCCAGGC	10	25	187.5	93.75
Vredmarkov167	GCCTGGGCGC	10	25	187.5	93.75
Vredtrans93	GGGGGCGCCG	10	25	187.5	93.75
10base00602	AGGCGATCAT	10	25	187.5	93.75

Optical spectroscopy: After synthesis of Ag_N-DNAs, we first measured Ag_N-DNA's absorbance and emission spectra using a variety of spectrometers. NIR emission was measured with a Tecan Infinite Pro 200 equipped with a custom InGaAs photodetector. This instrument measures emission intensity of Ag_N-DNAs from 700 nm to 1400 nm using 50 nm bandpass filters and is crucial to detect NIR nanoclusters with high intensities and in the NIR I and NIR II wavelengths, which are outside the range of most silicon-based commercial spectrometers. Ag_N-DNAs were excited at the DNA absorbance band between 280-320 nm for well plate measurements. Other instruments used include commercial UV/Vis and fluorescence spectrometer plate readers (Tecan Spark) and a custom spectrometer for single cuvette measurements, using a QE65000 spectrometer (Ocean Optics). This spectrometer measured absorbance from a DH-mini UV-vis-NIR light source at 1 second integration time. For fluorescence spectra, a UV LED light source was used for universal UV- excitation of the Ag_N-DNAs, using 10 second integration time for NIR samples.

Purification: An Agilent 1260 High-Performance Liquid Chromatography (HPLC) was used to purify the Ag_N-DNAs *(Fig. 1.2).* A core-shell C_{18} column was used as the stationary phase, and the mobile phase is a gradient of H_2O and MeOH with 35 mM triethyl ammonium acetate (TEAA) as an ion-pairing agent. Solvent gradients started with a high percentage of the aqueous solvent and slowly increase the percentage of MeOH during a 10 minute interval. The elution time depends on the difference in affinity of the sample to the stationary (apolar) and the mobile (polar) phase.

In-line detectors measure absorbance and emission of the eluant. The absorbance detector is set to collect at multiple wavelengths: 260 nm, the DNA absorbance peak, and the specific Ag_N-DNA absorbance features, as well as collecting a 3D map of full absorbance spectra from 250 – 900 nm as a function of time. The fluorescence detector can measure emission intensity at multiple wavelengths and full emission spectra. Before attempting to purify Ag_N-DNAs, we ensured their chemical yields were optimized (Chapter 2) and then prepared concentrated solutions using a Amicon 3k MWCO centrifuge filter. A Ag_N-DNA is considered pure when there is only one species in solution after purification, as evidenced by only one emission peak without spectral shoulders *(Fig. 1.3A).* To ensure reproducibility of chromatogram results, we found that it was important to run a MeOH wash of the column at the end of each day to clean the column of any residues.

Mass characterization: An electrospray ionization mass spectrometer (ESI-MS) from Waters Xevo G2-XS QTof was used to determine the chemical composition of the Ag_N-DNAs. Calibration was performed using 2 µg/L of cesium iodide (CsI). Samples went through three rounds of solvent exchange with NH_4OAc to remove residual HPLC buffer. Samples were injected using direct injection in negative ion mode (with a capillary voltage of 2 kV, cone voltage of 3V and no collision energy) with 50 mM NH_4OAc - MeOH (80:20) as injection buffers (pH 7) at 10 $\mu L \cdot min^{-1}$. To determine the size and charge of the Ag_N-DNAs, the experimental spectra were fitted to calculated isotopic distributions of varying cluster compositions and charges to determine the best match to experimental data (*Fig. 1.3B*).

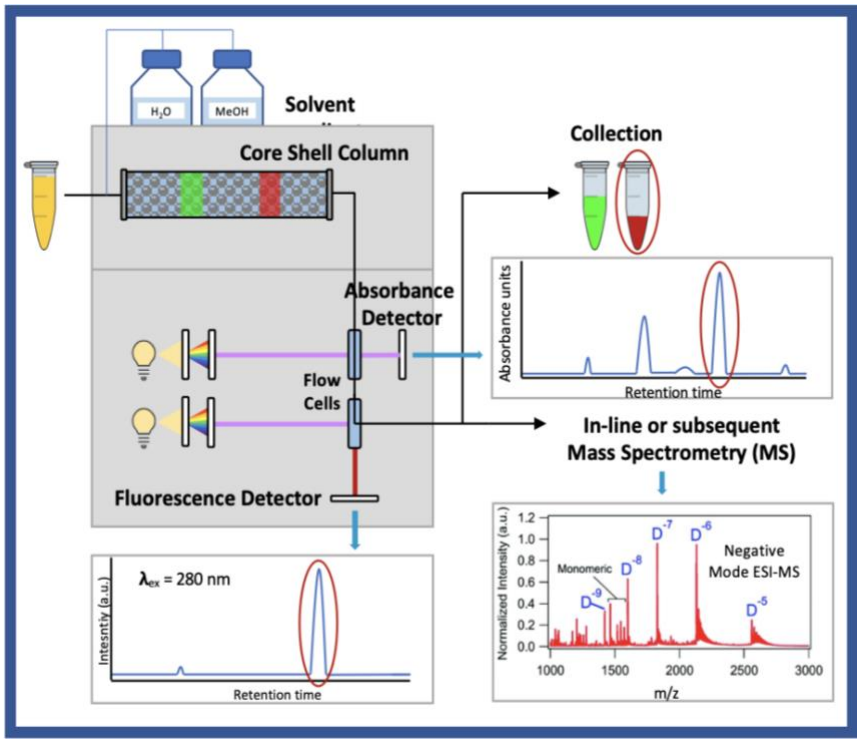

Figure 1.2. *HPLC schematics showing the different components of the instrument and resulting chromatogram.*[6]

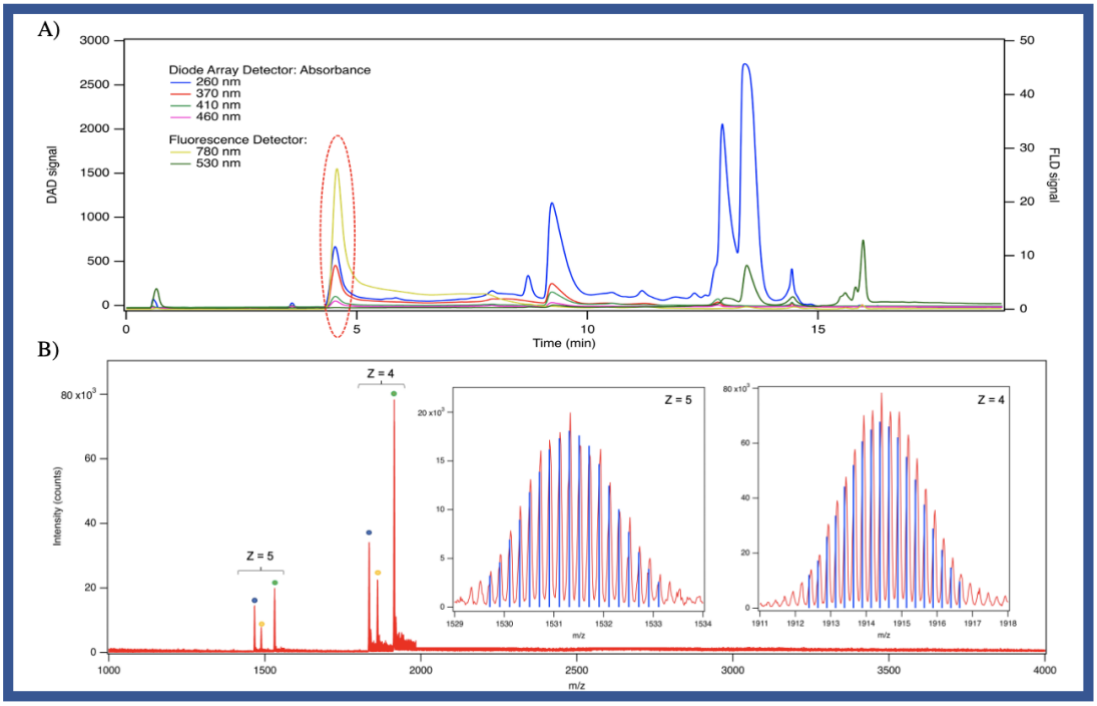

Figure 1.3. *An example of what purification and characterization results look like for GM18 shown through A) a chromatogram where the absorbance and fluorescence peaks align indication a pure 780 nm emission species and B) mass spectrometer isotopic distribution results signifying that the nanocluster has 2 DNA strands and 16 total silvers (green dots) with* $N_0 = 8$.[8]

Part 2

[Ag$^+$]:[DNA] stoichiometry sweeps: To optimize the chemical yield of an Ag$_N$-DNA synthesis, we performed silver concentration "sweeps" of 3.75, 5, 7.5, 10, 12.5, 15, and 20 times the DNA concentration. Ag$_N$-DNA were synthesized as described in Part 1, and fluorescence emission spectra were then collected at visible and NIR wavelengths, using UV light to universally excite all Ag$_N$-DNA products. Measurements were repeated 3, 5, and 7 days after synthesis to evaluate how the nanocluster products evolved with time as a function of synthesis stoichiometry. The stoichiometry consistent with the brightest intensity was utilized for future synthesis. Then DNA concentrations of 10, 15, 20, 25, 30, and 35 μM were "swept" to select the synthesis conditions best suited to increase chemical yield of the desired emissive product.

Results: The optimal stoichiometry concentrations determined for various Ag$_N$-DNAs are summarized in *Table 1.2* with an example of emission intensity results for TBG443 in *Figure 1.4.*

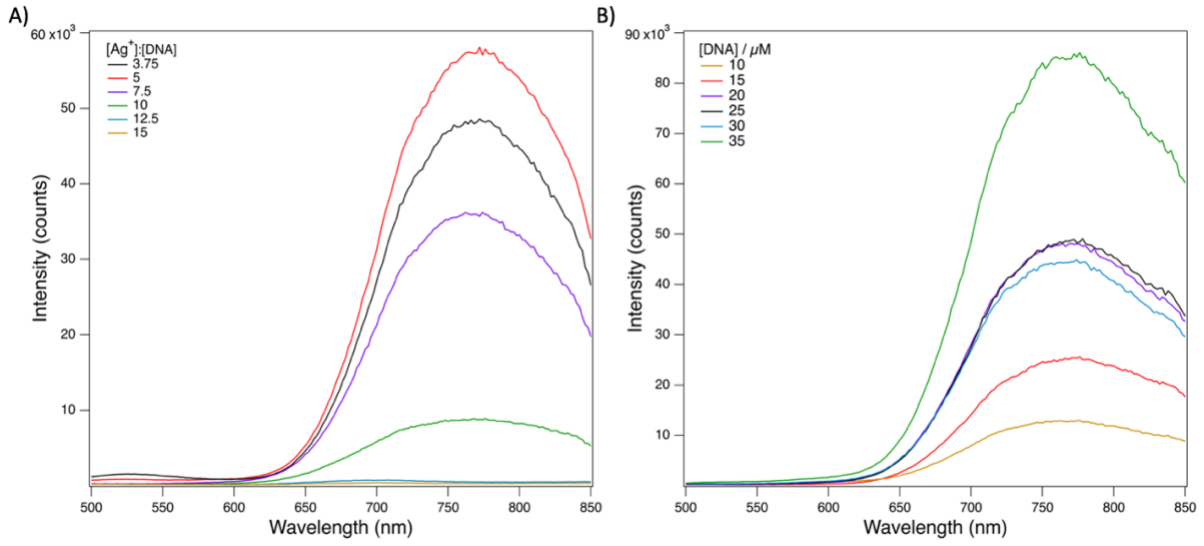

Figure 1.4. *Emission spectra of stoichiometry sweeps for TBG443 day 7 post synthesis where A) are the silver to DNA ratio is changed and B) at different concentrations of DNA, keeping the [Ag$^+$]/[DNA] ratio at 5.0. These graphs are used to determine the optimum concentration for silver cations and DNA to obtain highest chemical yield.*

Table 1.2. *[Ag^+]:[DNA] stoichiometry found to be optimal for yield of specific Ag_N-DNA species.*

Ag_N-DNA nickname	**Ag_N-DNA name**	**[Ag^+]:[DNA] stoichiometry**	**[Ag^+]:[DNA] stoichiometry for NIR peak**	**DNA concentration [μM]**
TBG443	10basegen443	5x	5x	35
TBG336	10basegen336	5x	5x	20
GG159	Greengen159	5x	5x	10
TBG59	10basegen59	7.5x	10x	20
TBG203	10basegen203	10x	15x	20
GT40	Greentrans40	10x	10x	20
TBG595	10basegen595	7.5x	7.5x	20

Part 3

Ag_N-DNA post-reduction temperature optimization: Ag_N-DNA species formation is initiated upon addition of $NaBH_4$, *i.e.* chemical reduction, followed by storage at 4°C. Using this method, the complete formation of NIR nanocluster species can take up to ten days. We have found that the temperature at which Ag_N-DNAs are stored after chemical reduction (referred to as "post-reduction temperature") can impact the evolution of the nanocluster products and speed up formation of NIR species. Based on this finding, experiments were conducted to determine the ideal temperature to store nanoclusters immediately after their synthesis. This was determined by

identifying what species increased in chemical yield and the time it took to fully form NIR-emissive Ag_N-DNAs. Three different time-dependent experiments were conducted at three different temperature environments after borohydride reduction: heating the reduced Ag_N-DNA solution at 37 °C, storing the reduced Ag_N-DNA solution at room temperature (21 °C), and keeping the reduced Ag_N-DNA solution at 4 °C. To heat the Ag_N-DNA solution, a hotplate was used where time duration and temperatures were set. Ag_N-DNAs stored at room temperature were wrapped in aluminum foil to protect from light exposure.

The first experiment examined changes in temperature variations over a short time span of 4 hours. Measurements were taken every hour to compare the absorption and intensity emission spectra. The second set of experiments evaluated how the Ag_N-DNA form over a longer period of time by measuring spectra once a day over the course of a week. Lastly, Ag_N-DNAs optical properties were evaluated after holding them at 37°C for up to four hours and then storing at either room temperature or at 4°C. Additionally, Ag_N-DNAs were mixed in a 1:1 ratio with sodium chloride (final concentration 0.9%), and the three sets of experiments were repeated to determine how temperature variations affect the nanocluster stability in saline solutions. A thorough evaluation of these findings are presented in chapter 3.

CHAPTER 2: Stabilizing Ag_N-DNAs in physiological conditions

It is important to develop methods to prevent Ag_N-DNAs from degrading in physiological salt conditions. DNA is known to have low stability in solutions with sufficiently high concentrations of divalent cations (including conditions relevant for biological systems) since the anionic phosphate backbone of DNA interacts strongly with these cations. Additionally, we have observed that addition of Ag_N-DNAs to a solution of saline or phosphate buffer saline (PBS) often causes Ag_N-DNAs to lose their luminescent properties. Thus, the first crucial step towards *in vivo* imaging applications requires developing strategies to allow Ag_N-DNAs to remain stable and bright in biologically relevant solutions and buffers. Different approaches have been explored for other types of DNA nanostructures to address this challenge.[15] We sought inspiration from a published method that uses various polyamines (oligolysine, spermine, and spermidine) to protect DNA origami nanostructures from degradation at physiological Mg^{2+} concentrations.[15] The electrostatic interaction between the positively charged polyamines, spermine and spermidine, and the negatively charged DNA strand encapsulating the Ag_N-DNAs could shield the nanocluster from solvent molecules and help prevent any degradation. However, polyamines are also known to deform DNA nanostructures when added in higher concentrations. Thus, we used low concentrations of polyamines with comparable sizes to the Ag_N-DNAs to preserve the structural integrity of nanoclusters.[15] We hypothesized that the polyamines spermine and spermidine, rather than oligolysine, would be more effective in protecting Ag_N-DNAs because these molecules are smaller than oligolysine and would be less likely to compromise the nanocluster's structural integrity.

Experimental Methods

Table 2.1. *Ag_N-DNAs specifications used for synthesis, their properties, and HPLC gradients needed to prepare and run the following experiments.*

Ag_N-DNA name	**Greengen268 (GG268)**	**Greenmarkov19 (GM19)**	**Greenmarkov18 (GM18)**	**Greengen322 (GG322)**
Sequence	CCCGGAGAAG	AGTCACGACA	ATCTCCACAG	CACCTAGCGA
Time between synthesis and HPLC (days)	5	3	5	5
HPLC Gradient (35 mM TEAA in H2O → MeOH), (0.10-12 min)	85-70%	88-73%	88-73%	80-65%
Phosphate number	27 (trimer)	27 (dimer)	18 (dimer)	18 (dimer)
Final Concentrations				
DNA [µM]	20	30	25	25
$AgNO_3$ [µM]	100	150	100	187.5
NH_4OAc [µM]	10	10	10	10
$NaBH_4$ [µM]	50	75	50	93.75

Ag_N-DNAs + polyamines Ag_N-DNAs were synthesized and purified using the HPLC gradients, listed in the *Table 1*, that had previously been optimized. Then, Ag_N-DNA concentration was measured using a Nanodrop UV/Vis spectrometer (the Nanodrop was found to work best when

calibrated with H_2O rather than 10 mM NH_4OAc). After entering the molecular weight of the DNA strand, the nanodrop outputted concentration ng/µL. To determine the concentration of DNA present in the Ag_N-DNAs, the coefficient of molar absorption was divided by the molecular weight in µM. Then, the concentration of Ag_N-DNAs was evaluated by dividing the concentration of DNA with the numbers of DNA strands stabilizing the nanocluster (Ag_N-DNAs can be stabilized by 1-3 strands of a DNA oligomer). Next, the ratio of the number of phosphates from the DNA to the number of nitrogens from the polyamines was identified (spermine has 4 nitrogens and spermidine has 3 nitrogens, see *Fig. 2.1*). These ratios were used to determine the concentration of polyamines needed to fully protect the Ag_N-DNAs.

The calculations were based on utilizing a well plate cell that would hold 40 µL of total solution (30 µL of the Ag_N-DNAs and 10 µL of a polyamine). This 40 µL solution had a final concentration of 5 µM of Ag_N-DNAs + *X* µM of a polyamine. Multiplying the number of phosphates in the DNA strand by 5 µM determined the final phosphate concentration. This value was then divided by the number of nitrogens from the polyamines. This generally led to diluting the Ag_N-DNAs to a 6.67 µM concentration from the concentration found using the Nanodrop. Next, the concentration of the polyamines was determined using the concentration and volume of the Ag_N-DNAs and the final 10 µL volume for a polyamine. Once all the concentrations were determined, the solutions were diluted as necessary. Three ratios of Ag_N-DNAs to polyamine concentrations (P:N = 1:0.5, 1:1, and 1:2.5) were tested in the well plates. This process was conducted for both polyamines, and samples were compared to a control: the Ag_N-DNA without a polyamine. Initial measurements were taken immediately after the polyamine addition, recording the emission intensity and absorbance spectra, and repeated periodically (2 and 5 days after mixing).

Ag$_N$-DNAs synthesis + polyamines + NaCl The stability of the Ag$_N$-DNAs with the polyamines was then tested in a saline solution. 20 µL from the well-plate solutions of Ag$_N$-DNAs with a polyamine was mixed with 20 µL of NaCl (0.9%) and added to a new well *(Fig. 2.1).* The control was mixed with 20 µL of ammonium acetate instead of NaCl. Measurements were then taken periodically.

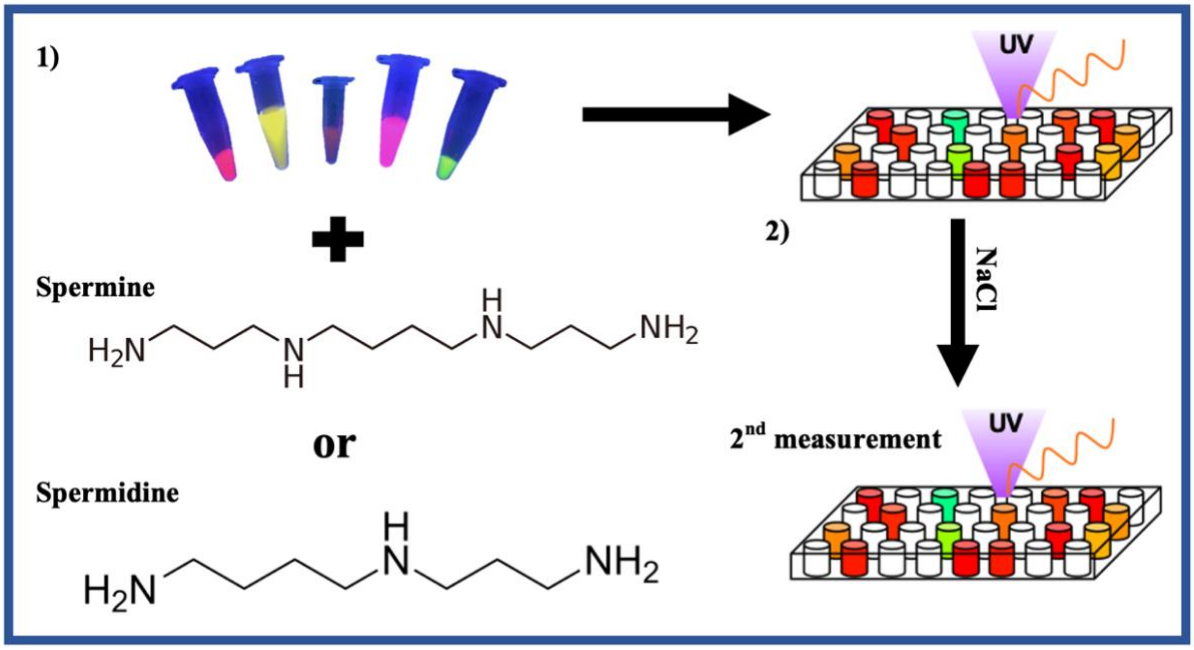

Figure 2.1. *Experiment schematic of Ag$_N$-DNAs with polyamines and sodium chloride mixture.*

Results

Two comparisons of Ag_N-DNAs absorbance and emission intensity spectra with polyamines were performed. First, we considered each Ag_N-DNA with each polyamine (spermine or spermidine). Second, we considered each Ag_N-DNA with the polyamines in the presence of NaCl. Our goal was to enable Ag_N-DNAs to increase or prevent a decrease in intensity for their emission peaks. The following results include two controls: 'Control 1' represents the Ag_N-DNA without a polyamine and sodium chloride. 'Control 2' is the Ag_N-DNA in the presence of sodium chloride but without a polyamine. Summarized findings indicate that neither spermine nor spermidine presented a consistent trend when combined with the Ag_N-DNAs and ultimately did not aid in stabilizing the nanocluster (with or without sodium chloride). It is concluded that in some cases, the polyamines quench the Ag_N-DNAs emission without affecting their excitation spectrum.

We first tested the effects of polyamine protection on GG322 *(Fig. 2.2A),* which was the only nanocluster known at the time to remain stable in saline solutions. The goal of studying this Ag_N-DNA was to establish understanding of how the nanoclusters interact with the polyamines. For cases in *Figures 2.2B-2C and 2.2F-2G*, control 1 is brighter than any of the P:N ratios demonstrating that the polyamines don't help increase or keep the intensities the same brightness as the Ag_N-DNA alone. On the other hand, when evaluating the corresponding absorbance spectrum in *Figure 2.2C*, day 2 increases compared to day 1, but control 1 has the largest absorbance. GG322 does appear to increase in stability in *Figure 2.2E* when spermine and NaCl are added as the P:N ratios have slightly higher or the same intensities than control 1 and 2, although day 2 significantly decreases below day 0. Yet for all these cases, there is at least one P:N ratio that is greater than control 2, which could signify that the polyamines are helping stabilize the nanocluster in NaCl. However, this cannot be confirmed because the results are not very clear

or reproducible for other species of Ag_N-DNAs. Lastly, we note that the emission for day 2 significantly decreases in intensity compared to day 0 for all cases.

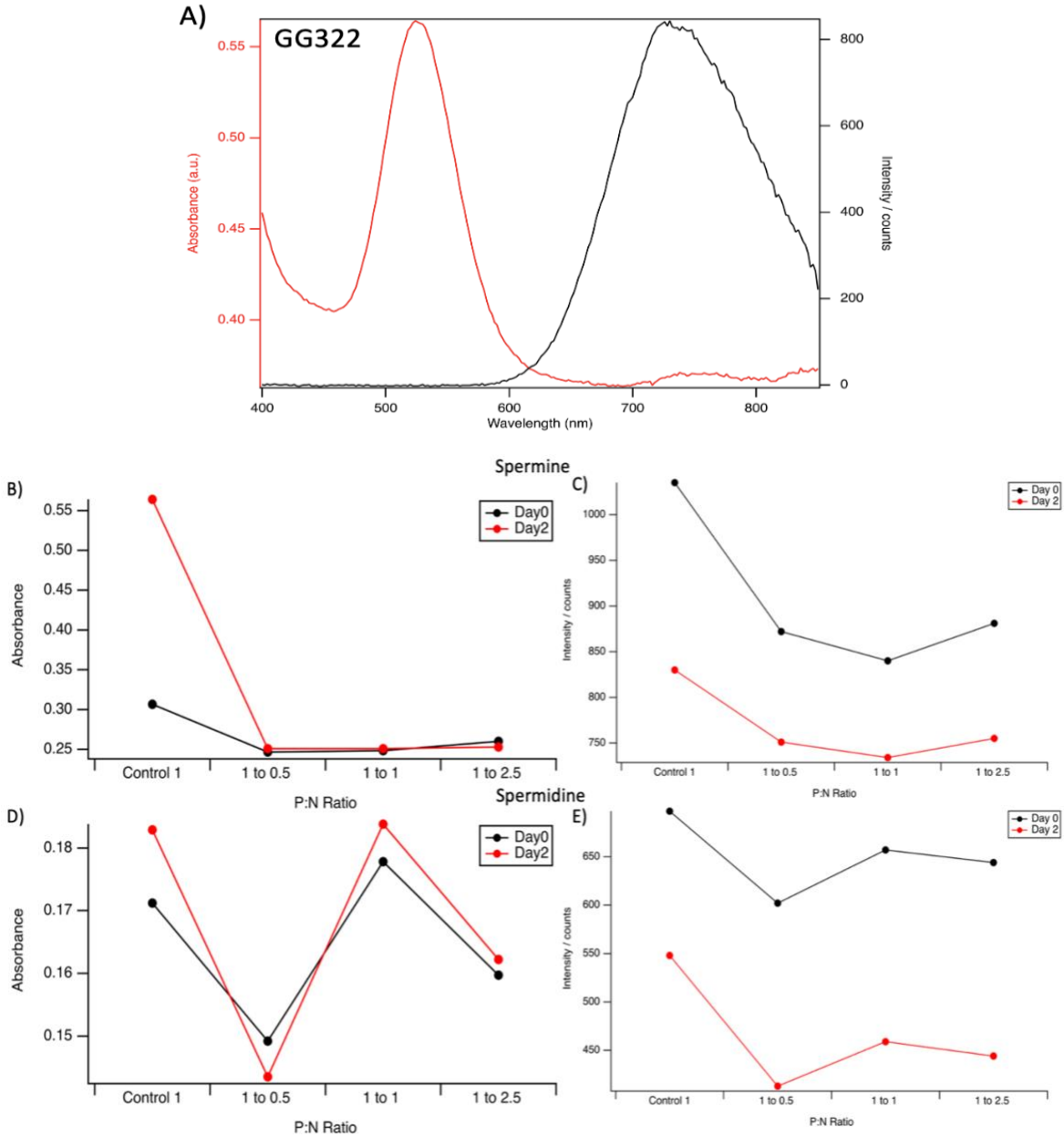

Figure 2.2. *GG322 experimental results comparing absorbance and emission intensity without any NaCl. Absorbance graphs on the left-hand side are at 524 nm peak and emission graphs on the right side are at 740 nm peak. 'Control 1' represents 20 µL of GG322 without polyamines + 20 µL* NH_4OAc *(10µM). A) GG322 absorbance and emission spectra B) GG322 absorbance with spermine C) GG322 emission with spermine D) GG322 absorbance with spermidine E) GG322 emission with spermidine.*

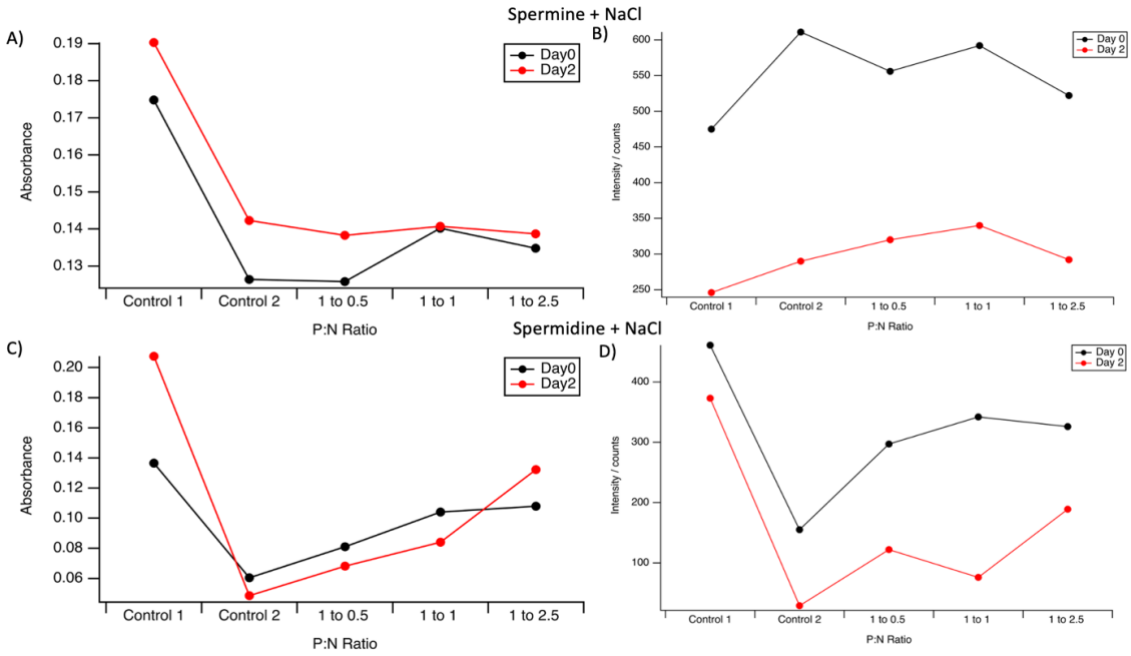

Figure 2.3. *GG322 experimental results comparing absorbance and emission intensity with NaCl. Absorbance graphs on the left-hand side are at 524 nm peak and emission graphs on the right side are at 740 nm peak. 'Control 1' represents 20 µL of GG322 from Control 1 in Fig. 2 + 20 µL* NH_4OAc *(final = 5 µM). 'Control 2' represents 20 µL of GG322 from Control 1 in Fig. 2 (already includes 10 µM* NH_4OAc*) + 20 µL* NaCl *(final= 5µM). A) GG322 absorbance with spermine and NaCl B) GG322 emission with spermine and NaCl C) GG322 absorbance with spermidine and NaCl D) GG322 emission with spermidine and NaCl.*

Unlike GG322, GG286 demonstrated clearer trends of not remaining stable and bright in the saline buffer from the addition of the polyamines. Notably, GG268 emission intensity is completely quenched on day 1 for both spermine and spermidine in the presence of NaCl, while the absorbance only slightly decreased (*Fig. 2.3D-E, 2.3H-I)*. The fact that Ag_N-DNA luminescence was quickly quenched shows that the polyamines were not able to protect the Ag_N-DNA in saline conditions, but the persistence of the absorbance peak suggests that the nanocluster is not destroyed but rather just quenched by the spermine and spermidine. This can also be seen where some P:N ratios may survive and even increase intensity compared to control 1 for day 0, but emission then diminishes through day 2 (*Fig. 2.3E, G)*.

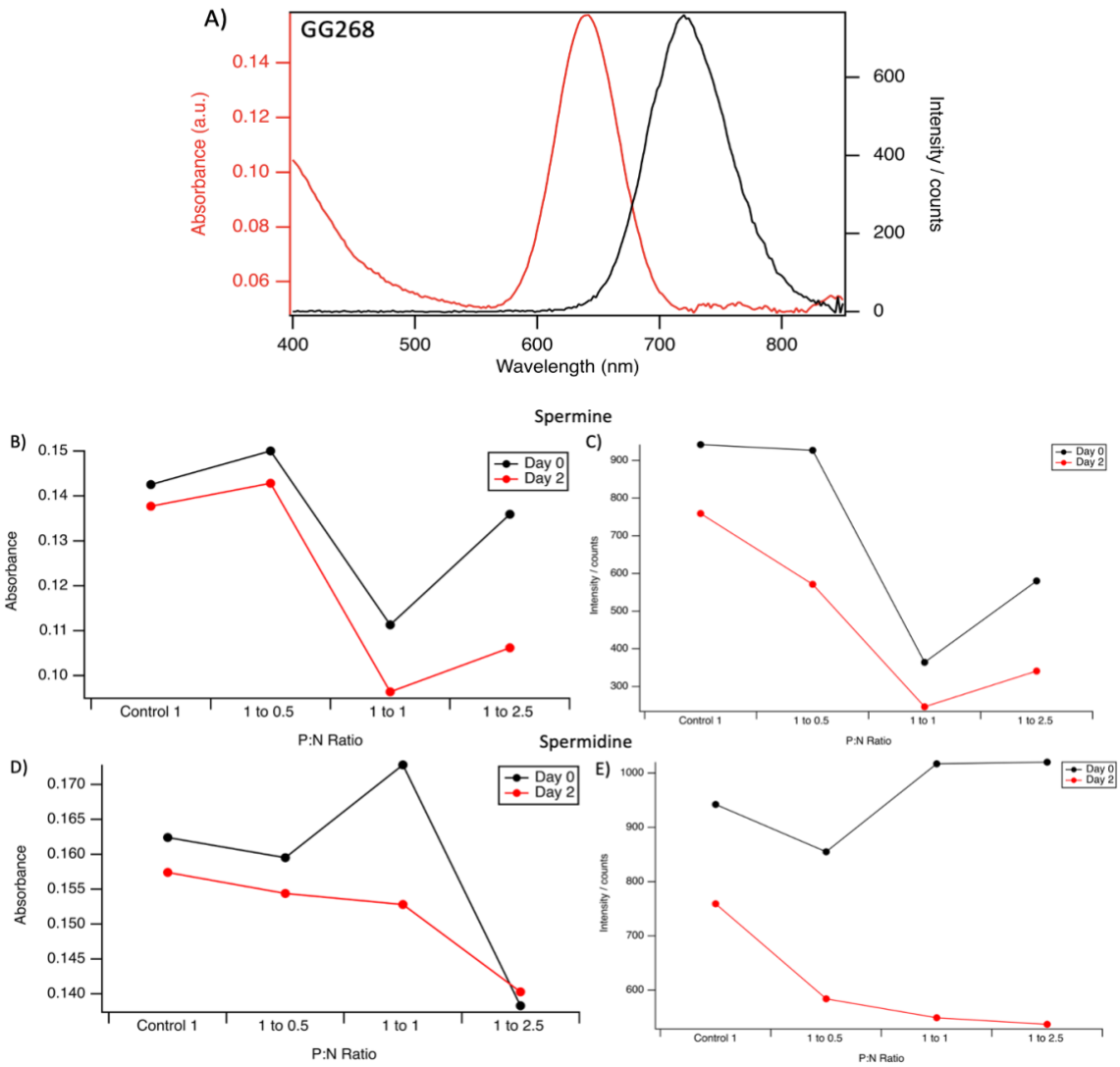

Figure 2.4. *GG268 experimental results comparing absorbance and emission intensity without any NaCl. Absorbance graphs on the left-hand side are at 524 nm peak and emission graphs on the right side are at 740 nm peak. 'Control 1' represents 20 µL of GG268 without polyamines + 20 µL* NH_4OAc *(10µM). A) GG268 absorbance and emission spectra B) GG268 absorbance with spermine C) GG322 emission with spermine D) GG268 absorbance with spermidine E) GG268 emission with spermidine.*

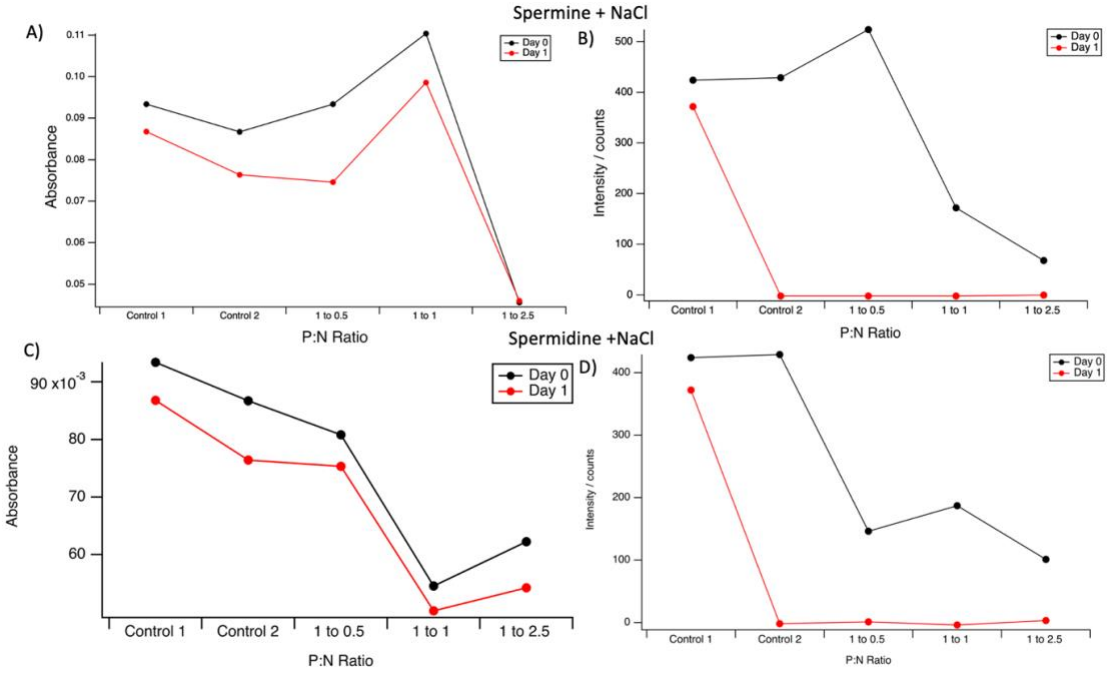

Figure 2.5. *GG268 experimental results comparing absorbance and emission intensity with NaCl. Absorbance graphs on the left-hand side are at 524 nm peak and emission graphs on the right side are at 740 nm peak. 'Control 1' represents 20 µL of GG268 from Control 1 in Fig. 2 + 20 µL* NH_4OAc *(final=5µM). 'Control 2' represents 20 µL of GG268 from Control 1 in Fig. 2 (already includes 10 µM* NH_4OAc*) + 20 µL* NaCl *(final= 5µM). A) GG268 absorbance with spermine and NaCl B) GG268 emission with spermine and NaCl C) GG268 absorbance with spermidine and NaCl D) GG268 emission with spermidine and NaCl.*

Although some cases presented an insignificant increase/consistency in emission, the overall the goal of increasing Ag_N-DNAs stability in saline conditions using polyamines was not attained in this chapter. Results for GM18 and GM19 are not presented because for both Ag_N-DNAs, the fluorescence was quenched on day 0 by addition of spermidine and spermine. We were unable to perform protection experiments with oligolysine because our collaborator provided less oligolysine than needed. Other studies show that oligolysine appears to be more effective in some cases than the polyamines for protecting DNA origami from degradation, so future studies should experiment with oligolysine protection of Ag_N-DNAs.[15] Additionally, future studies should also include experiments with varied temperature mixing conditions for protecting Ag_N-DNAs with polyamines, as some studies perform this protection under heating to 37 °C.[15] Lastly, we suggest

that a wider range of P:N ratios should be screened, since some cases found very high concentrations of polyamines were needed for full protection of DNA nanostructures from denaturation.[15] In the following chapters, Ag_N-DNAs are tested in physiological conditions without adding any protecting macromolecule and we report that specific Ag_N-DNAs can remain stable on their own without such protection.

CHAPTER 3: Determining optimal post-reduction temperature conditions for Ag_N-DNAs

The standard method of Ag_N-DNA synthesis, first introduced by Petty, *et al.*, in 2004,[16] is to store reduced solutions of DNA and silver at 4 °C (in a standard laboratory refrigerator) while the nanocluster species form. By this method, we found that NIR-emissive Ag_N-DNAs can take up to 9 days to reach their peak intensity emission, and even then, are often not very bright, suggesting very low chemical yield of the fluorescent nanocluster species. Our motivation for exploring the post-reduction temperature of Ag_N-DNAs as a route to increase this chemical yield stemmed from noticing a discrepancy in the results of high-throughput experiments and individually synthesized nanoclusters. High-throughput experiments utilized an automated robot pipetting system and automated well plate reader to synthesize and spectrally characterize a well plate of 384 specific Ag_N-DNAs. Well plates were synthesized one week before fluorimetry, with preliminary fluorimetry performed one day after synthesis. The lengthy process of fluorimetry of 384 Ag_N-DNAs to collect 400 – 850 nm emission spectra and then NIR fluorescence intensities[17] of each well means that the well plate is kept at room temperature for nearly 8 hours before being returned to 4 °C on day 1 and day 7 after synthesis. This exposure to room temperature is significantly different than when the Ag_N-DNAs are individually synthesized and only removed from refrigeration for short periods of time for optical characterization. Therefore, we hypothesized that the differences between the fluorescence emission spectra of some Ag_N-DNAs synthesized in high throughput as compared to individual tubes was due to the post-reduction environmental temperature conditions the Ag_N-DNAs were stored at for extended periods of time.

We found that increasing the post-reduction temperature following chemical reduction can significantly increase the chemical yield of Ag_N-DNAs and decrease the time required for nanocluster formation, especially for NIR-emissive nanoclusters (*Table 3.1*). The optimal post-reduction temperature conditions vary depending on the Ag_N-DNA species but storing NIR-emissive nanoclusters at room temperature was found in most cases to be very effective in increasing the intensity as well as decreasing the overall time of formation to around 3-4 days. For example, consider TBG354, an Ag_N-DNA species that emits at 620 nm and has a lesser product at 830 nm (*Fig. 3.1A*). We found that storing TBG354 at room temperature after chemical reduction caused a dramatic 50-fold increase in the intensity of the 830 nm product, which became the dominant product (*Fig. 3.1C*). The effects of post-reduction temperature were greater for the NIR-emissive product than for the visibly emissive product (*Fig. 3.1B*). This result shows that temperature plays an especially important role in the chemical synthesis of NIR-emissive Ag_N-DNAs and that temperature may be a promising parameter to vary in order to achieve high yields of Ag_N-DNAs for NIR bioimaging applications.

Table 3.1. *Summary of optimal post-reduction temperature conditions found for various Ag_N-DNA species, the time required to reach brightest intensity, and whether temperature conditions increase their stability in NaCl.*

Ag_N-DNA nickname	**Ag_N-DNA name**	**Optimal post-reduction temperature conditions**	**Length of required days to reach optimal formation (days)**	**Temperature treatment effect on stability in NaCl**
TBG354	10basegen354	Room Temperature	3-4	
TB419	10base419	Room Temperature	3-4	
TBG59	10basegen59	Heated at 37°C	3	
GT40	Greentrans40	Room Temperature	3-4	
TBG203	10basegen203	Room Temperature	3-4	
TBG66	10basegren66	Heated for 4hr at 37°C, then stored at room temperature	3-4	
Petty900	Petty900	Room Temperature	3	

GG77	Greengen77	Room Temperature	3	
TBG595	10basegen595	Room Temperature	7	
TB00384	10base00384	Room Temperature	3-5	
VRM167	vredmarkov167	Room Temperature	3-5	
VRT93	vredtrans93	Heated for 4hr at 37°C, then stored at room temperature	3-5	
TB00602	10base00602	Heated for 4hr at 37°C, then stored at 4°C	3-4	
VRM42	Veryredmotif42	4°C after adding NaCl	2	Only stable at 4°C
VRMM95	Veryredmotifmarkov95	Room Temperature	1	Only survives for 1 day

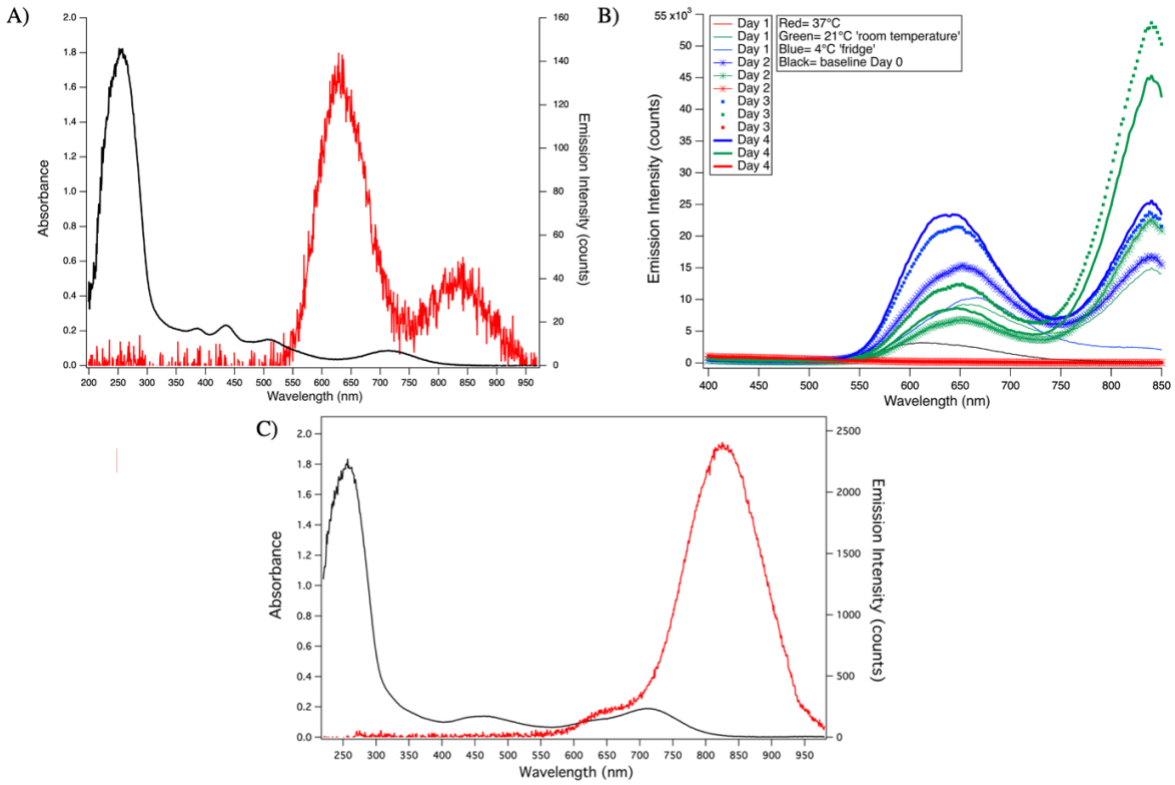

Figure 3.1. *Change in chemical yield of TBG354 as a function of post-reduction temperature. A) Day 7 post-synthesis absorbance and emission spectra for samples stored continuously at 4 °C following chemical reduction. B) The effects of 37 °C, 21 °C, and 4 °C post-reduction temperatures are compared by measuring emission spectra on days 1-4 following reduction. C) Day 3 post-synthesis absorbance and emission spectra of TBG354 stored at room temperature (note: A and B were taken with the same spectrometer at 10s integration, allowing direct comparison of their intensity counts, whereas B) was taken with a different spectrometer).*

We also found that varying the post-reduction temperature of Ag_N-DNAs can influence the formation of different nanocluster species in solution. In some cases, completely different Ag_N-DNA species formed, with different absorption and emission peaks, due to post-reduction temperature. In conjunction with the aforementioned results, storing Ag_N-DNA at room temperature appears in most cases to be the optimal to form NIR-emissive species rather than a red species typically formed by storing the nanoclusters at 4 °C. Additionally, we noticed that heating Ag_N-DNAs to 37 °C can either increase the overall emission intensity or completely hinder nanocluster formation. The best results with heating were achieved when the Ag_N-DNA was only

kept on the hot plate at 37 °C for four hours and then stored for the remainder of the duration at room temperature or at 4 °C.

For example, the DNA template strand TBG66 forms a new NIR-emitting nanocluster that is completely absent prior to elevating temperature following chemical reduction. The original 680 nm peak is diminished, and an 820 nm peak with higher emission intensity appears after heating the reduced DNA-Ag^+ solution at 37°C for 4 hours and then storing it at room temperature (*Fig. 3.2*). We also observed that storing the Ag_N-DNA species at room temperature or heating at 37°C for 4 hours and then storing at 4°C forms the new NIR nanocluster species but with less yield than when stored at room temperature following 4 hours of heating at 37 °C. Not only did we discover this new NIR-emitting nanocluster, but the nanocluster has a very high intensity and forms within only one day after chemical reduction. Before this experiment was conducted, TBG66 was never considered a candidate template sequence for NIR Ag_N-DNAs, making this discovery especially surprising. This result is a promising indication that there could be many new NIR-emissive Ag_N-DNAs that can easily be identified by increasing the temperature following chemical reduction. We also found that Ag_N-DNAs do not need to be stored at 37°C for a long period of time to make a substantial difference in NIR nanocluster formation.

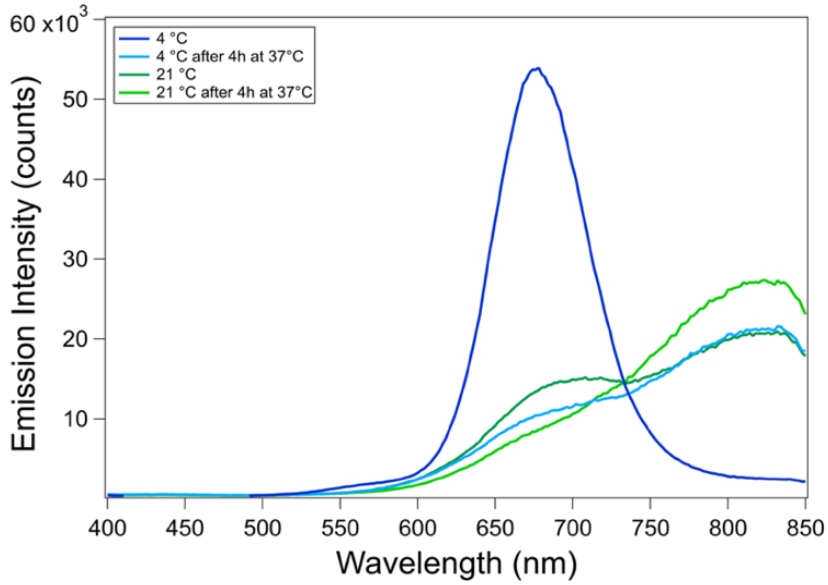

Figure 3.2. *Emission spectra of TBG66 stored at 37 °C, 21 °C, and 4 °C. Spectra were collected 1 day post synthesis.*

To further explore the temperature effects on the formation of Ag_N-DNAs, we aimed to determine if initial post-reduction effects on species formation at one temperature can be altered by changing the temperature later in the species formation process. TBG66 is a perfect candidate for this experiment as it forms one bright red species when stored at 4°C and a completely different NIR species if kept at higher temperatures. We stored the newly reduced Ag_N-DNA at 4°C from day 0 until day 3. On day 3, we saw that TBG66 started to form a NIR spectral shoulder when kept at these colder temperatures, while the red product dominated. In an attempt to reverse the formation of the red species and only form the NIR peak, (similar to what we achieved in *Figure 2* from heating the nanocluster at 37°C and then storing at room temperature) we then stored the nanocluster at room temperature from days 3-5. This caused the NIR peak to grow and the red peak to decrease in intensity over time *(Fig 3.3A).* We found that the post-reduction conditions not only affect species formation initially, seen when originally isolating the NIR peak, but that changing the temperature condition can also completely alter nanocluster species that have already

formed. We repeated this experiment with the Ag_N-DNA stabilized by DNA sequences TB00384 (*Fig. 3.3B*) and TBG354 and observed similar effects.

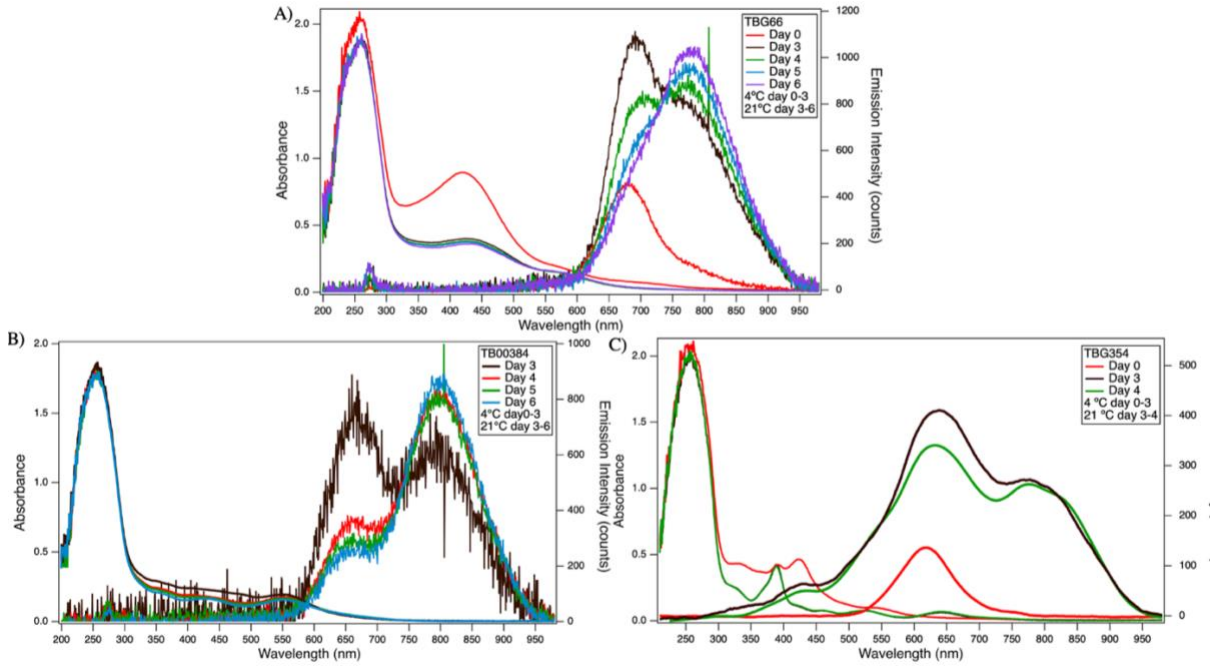

Figure 3.3. *Absorbance and emission spectra of A) TBG66 and B) TB00384 C) TBG354 after being stored at 4 °C from days 0-3 and then at room temperature from days 3-6.*

This study also aimed to evaluate multiple circumstance by first determining how nanocluster stability is affected by altering the temperature environment at which Ag_N-DNAs are mixed with saline and when saline is added by focusing on the first 4-hour post synthesis. Two Ag_N-DNAs were chosen for these tests, which had previously shown stability against saline in high-throughput experiments but did not show the same stabilities against saline when individually tested. The first Ag_N-DNA, VRM42, was stable in saline, but the emission peak blue shifted from around 690 nm to 504 nm with the addition of NaCl. Our goal was to determine if the same 690 nm species could remain stable after the addition of NaCl by trying the three different temperature environments. The results show that changing the post-reduction temperature did not prevent the blue shift in

species formation, but it did increase the brightness of the new 504 nm species formed from the addition of NaCl. NaCl was added prior to and after 4 hours at the different temperature treatments. We found that heating the Ag_N-DNA at 37°C yielded the brightest 504 nm species (*Fig. 3.4B.)* when NaCl was added after 4 hours whereas NaCl added prior to storing the nanocluster at 4°C (*Fig. 3.4A)* caused the intensity at 504 nm to become almost 2 times greater. It is important to note that these comparisons were made with two different Ag_N-DNA syntheses, so the reference samples (the nanocluster without NaCl) indicated by the solid lines in *Figure 3.4A, B* have two different intensities.

Next, the stability of Ag_N-DNAs in NaCl solution was evaluated for two days to study the progression of species formation over a longer period. Results indicate that although varying post-reduction temperature was not successful in preventing a change of species formation for VRM42 from the addition of NaCl, we were able to increase intensity of the new species. After the initial 4-hour measurements, VRM42 was either left for a 2-day period at the same temperature it was held at for the first 4 hours (its respective temperature), or it was placed in the refrigerator at 4°C (Note: samples were only stored at their respective temperature and not stored in the refrigerator for the case where NaCl is added prior to temperature treatments). Day 1 results showed the greatest difference in intensity when NaCl is added after 4-hour temperature treatment and the Ag_N-DNA is stored at 4°C (*Fig. 3.4D*). In comparison, heating the Ag_N-DNA for 1 day caused the brightness to decrease for both cases (*Fig. 3.4C, D*). Day 2 results verify that for this VRM42, post-reduction at 4°C is optimal for nanocluster stability in saline as it increases the intensity of the blue species. Results also indicate that adding NaCl after 4 hours leads to higher intensities for a longer time, although initially adding NaCl after synthesis yields a higher intensity at the 4 hour mark.

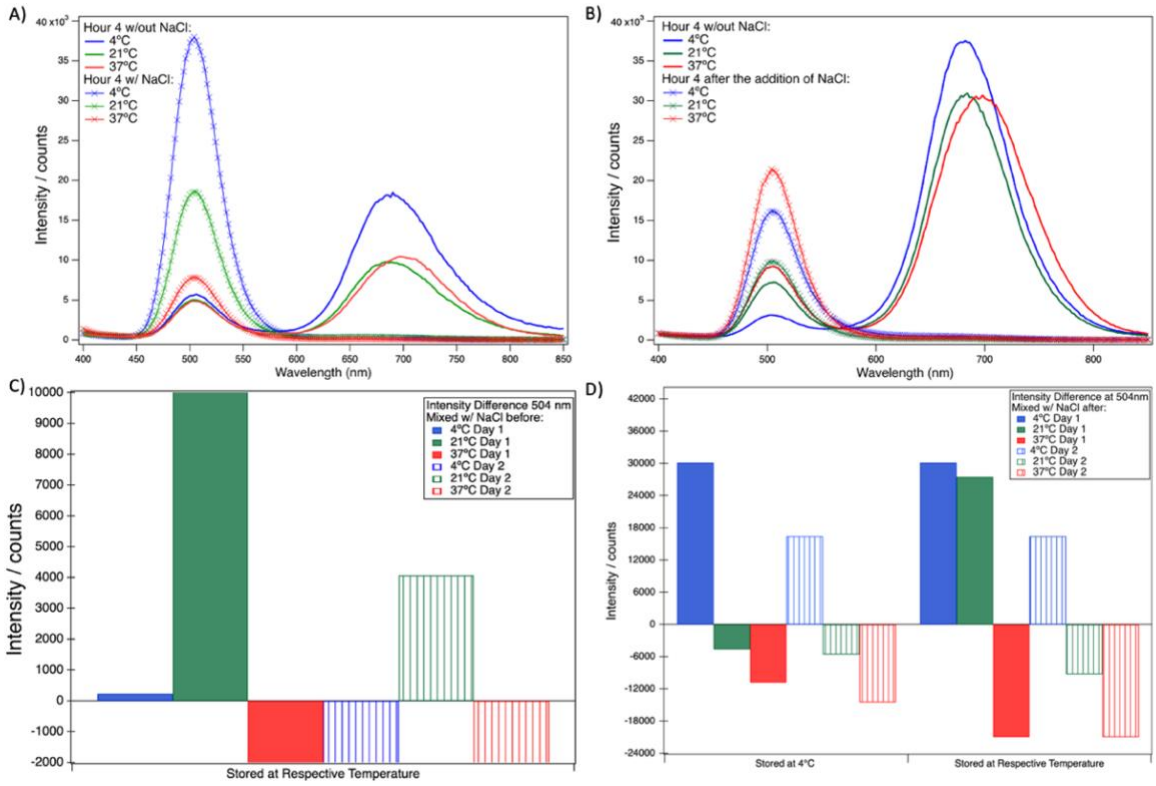

Figure 3.4. *Effects of post-reduction conditions and the timing of adding NaCl on* VRM42's *stability in NaCl. A) Emission spectra taken at the four-hour mark after mixing VRM42 with NaCl before the temperature treatments (case 1) indicated by the lines with x's, and without NaCl (as references) indicated by solid lines at 37°C, 21°C, and 4°C B) Emission spectra measured for VRM42 following temperature treatments for four hours and then mixing with NaCl (case 2) indicated by the lines with x's, and without NaCl (as references) indicated by solid lines at 37°C, 21°C, and 4° C C) Emission intensity differences for the 504 nm species after storing at the respective temperatures for 1 and 2 days for case 1 where NaCl was added prior to 4 hour temperature treatments. D) Emission intensity differences for the 504 nm species after storing at the respective temperatures vs 4 °C for 1 and 2 days for case 2 where NaCl was added after the 4 hour temperature treatments.*

The last part of this study investigated whether changes in post-reduction temperature could elicit the same Ag_N-DNA stability in saline that was originally seen in the high-throughput experiments but could not be reproduced on the individual level. Without the addition of NaCl, this Ag_N-DNA, VRMM95, displayed bright and stable emission spectra after 4-hour temperature treatments as seen in *Figure 3.5A* indicated by the solid lines. NaCl was then added after the 4-hour temperature treatments and the emission was quickly quenched (indicated by the lines with x's in *Figure 3.5A*). The nanocluster mixed with NaCl was then placed at 4°C or left at its respective temperature with

measurements taken on days 1 and 2. Although the emission was originally quenched, the nanocluster species was found to be stable in saline on day 1 with an increase in emission after being stored at room temperature, as shown in *Figure 3.5B (*green curve with x's*).* This result is interesting because VRMM95 then had a negative difference in emission intensity on day 2 indicating no fluorescence although day 1 had emission (*Fig. 3.5C*). Therefore, we were successful in discovering a post-reduction temperature condition that aided in stabilizing the Ag_N-DNA in saline while noting it was only for 1 day. Storing the Ag_N-DNA at room temperature proves again to be a critical in amplifying chemical yield and therefore increasing brightness of Ag_N-DNAs.

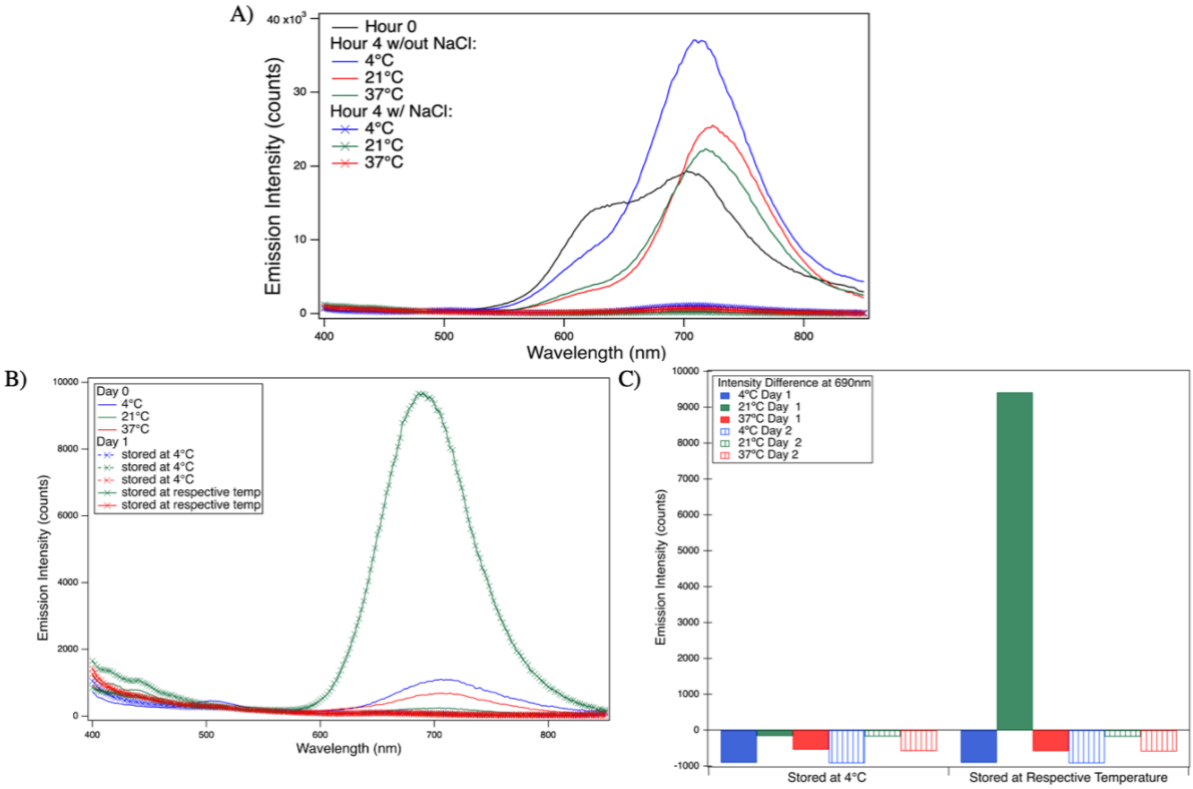

Figure 3.5. *Effects of post-reduction conditions of stabilizing VRMM95 in NaCl A) Emission spectra measured following temperature treatments for four hours and then mixing with NaCl (case 2) indicated by the lines with x's, and without NaCl (as references) indicated by solid lines at 37°C, 21°C, and 4° C compared to hour 0 before temperature treatments (black line) B) Emission spectra after storing at the respective temperatures vs at 4° C for 1 day C) Emission intensity differences for the 690 nm species after storing at the respective temperatures vs at 4 °C for 1 and 2.*

Overall, this chapter illustrates how post-reduction temperature conditions were found to be crucial in the formation of new NIR-emissive species, increasing the emission intensity and decreasing the overall time to fully form a species. The original method of storing all Ag_N-DNA at 4 °C proved to rarely be the optimal post-reduction condition needed. The two newly discovered temperature treatments that were most effective were storing Ag_N-DNA immediately after chemical reduction at room temperature or heating the nanocluster for 4 hours at 37 °C and then storing at room temperatures. Lastly, Ag_N-DNAs stability in saline was not drastically affected by post-reduction temperature conditions, although in some cases it did aid in increasing emission intensity. The exact correlation between post-reduction temperature and species formations is still unknown, but for most causes, storing NIR-emissive species at room temperature appears to increase chemical yield. To further optimize chemical yield of Ag_N-DNAs, our results support that it is appropriate to try four different post-reduction temperature conditions: 4 °C, 21 °C, 37 °C for 4 hours + the remainder of the time at 21 °C or 4 °C. The significant implications of these findings are further illustrated in the following chapters because these methods enabled Ag_N-DNAs to be scaled up, purified, and compositionally characterized by mass spectrometry.

CHAPTER 4: Purification and characterization of NIR-emissive Ag_N-DNAs

Only a few NIR-emissive Ag_N-DNAs are reported to have been successfully purified and sized by mass spectrometry.[18] To develop these emitters for applications in bioimaging, it is important to better understand and develop Ag_N-DNAs with high-intensity emission in the NIR I and II windows. Thus, there is a need to identify HPLC-purifiable NIR-emissive Ag_N-DNAs. Characterizing a larger set of NIR-emissive Ag_N-DNAs will improve the understanding of how their size (numbers of DNA strands and silver atoms per nanocluster) and the fraction of silver atoms that are positively charged correlate to their photophysical properties. It is equally important to determine the stability of NIR-emissive Ag_N-DNAs in NaCl to ensure that these nanoclusters are fluorophores applicable for bioimaging. This chapter reports the successful purification and characterization of three NIR-emissive Ag_N-DNAs, TBG354, TBG66, and TBG203 and their stabilities in saline solution.

Purification of Ag_N-DNAs can be a challenging task because these nanoclusters can be unstable in the HPLC, and their HPLC elution profiles are unpredictable. Promising NIR-emissive Ag_N-DNAs were identified using the high throughput experiments and machine learning models.[13] We specifically focused on nanoclusters that emit in the 800-900 nm region with bright intensities and aim to later explore nanoclusters in the NIR II window. HPLC purification conditions for each Ag_N-DNA were determined by screening numerous MeOH gradients, interval times, flow rates and other parameters. Determining the right environment to separate all but one species from a crude Ag_N-DNA sample takes bulk synthesis and many HPLC iterations. Additionally, Ag_N-DNAs often to have multiple species in solutions with absorbance peaks close in wavelength, which requires separating multiple emissive species from one another.

Characterization of composition for purified Ag_N-DNAs was achieved using electrospray ionization mass spectrometry (ESI-MS) in negative mode. ESI-MS aids in determining the size of the Ag_N-DNA, including the total number of DNA strands and silvers in the nanocluster, as well as the charge of the cluster, *i.e.*, the number of neutral and cationic silvers. By this method, we aim to understand whether there are trends that correlate the composition and spectral properties of NIR-emissive Ag_N-DNAs and to better understand their chemical and photophysical properties.

The final step in determining whether a Ag_N-DNA, that could be purified, is a suitable fluorophore for bioimaging is to test the nanocluster's stability, *i.e.* luminescence, in the presence of NaCl. The unpurified Ag_N-DNAs were mixed in a 1:1 ratio with NaCl (20 µL of Ag_N-DNA with 20 µL of 0.9% NaCl in a well plate cell) with spectra measurements taken over the course of a few days. Ag_N-DNAs with emission intensity that remained stable in the saline are promising candidates for future optical microscopy applications as well as *in vivo* mice toxicity and stability experiments.

Results

Table 4.1. *Summary of all Ag_N-DNAs that were attempted to be purified, including their peak excitation and emission species and why HPLC purification may have failed. The three Ag_N-DNAs bolded with an asterisk were successfully purified.*

Ag_N-DNA nickname	**DNA Sequence (5'-3')**	**Can it be purified by HPLC?**	**Peak Excitation (nm)**	**Peak Emission (nm)**
Petty900	CCCACCCACCCACCCG	Abs. chromatogram peaks are too close to separate species with different emission peaks	850	910
10basegen354*	CGAACCGGGC	Yes	709	811
10base00419	ACCTGGACCG	Abs. chromatogram peaks are too close to separate species with different emission peaks	610	720
Greenmarkov119	AATAACCCAC	No	530	790
Greentrans77	GGACAAAGAC	Yes, but isolated elution fractions shift between the 750 and 800 nm emission peaks	700	800
10base00222	TCGTTCAAGG	No	600	785
Greengen313	CCAAGAATAG	No	500	780
10base00572	ATTCTTCTTG	Possibly, but not bright enough to be able to identify a pure species.	710	845
allten699153	GGGGGTACAA	No	600	800
allten50453	AATACCACCA	No	600	750
10basegen151	ATCCCACCTC	No	580	650
allten698369	GGGGGAAAAA	No	550	800

allten698433	GGGGGACAAA	No	570	775
Greentrans40	GATCTAGACC	Sometimes but the intensity is too low, and the Abs. chromatogram peaks could be better separated	630	820
10basegen59	ACCCGGCGCG	Possibly but not optimized yet, worth trying again	800	850
10basegen66*	ACCGCCGGGA	Yes	580	784
10basegen203*	CACCCCGAGC	Yes	580	685
10basegen336	CCGTCCCGCC	No	550	710
10base00384	GGGGCCAGGC	Possibly but the Abs. chromatogram peaks could be better separated	650	820
10base00602	AGGCGATCAT	Possibly but the Abs. chromatogram peaks could be better separated	575	820

TBG354: the importance of monitoring HPLC purification conditions

This nanocluster species illustrates how HPLC conditions for purification of Ag_N-DNA species can vary over months. TBG354, stabilized by with a DNA oligomer with sequence 5'-CGAACCGGGC-3', presents an emission wavelength at 811 nm with two absorbance peaks at 625 nm and 709 nm and a lesser peak at 441 nm (*Fig 4.1*). This nanocluster was synthesized with final concentrations of 20 µM DNA, 10 mM NH_4OAc, 187.5 µM $AgNO_3$, and 93.75 µM $NaBH_4$. There are some important details to note about the purification process of TBG354. Firstly, two different HPLC gradients and chromatogram trends were exhibited for this nanocluster. Initially, an 85-75% aqueous-to MeOH gradient demonstrated a consistent chromatogram, with the Ag_N-

DNA eluting around 6 min (*Figure 4.2A*). This gradient was determined after many trials and was found to best separate the 811 nm emissive species from the 625 nm emissive species. However, we found that a few months later, these same HPLC conditions were no longer sufficient for purification. Instead, we found that a 90-75% gradient was sufficient, with the 811 nm species eluting around 8 to 9 minutes (*Fig. 4.2B*). This change in the gradient does not change what percent of MeOH the 811 nm species elutes at. It is uncertain whether degradation of the HPLC column required us to change the HPLC conditions, but our findings illustrate the importance of testing HPLC conditions regularly and between instruments to ensure proper purity of nanocluster species. Additionally, absorbance spectra differences between various purified samples suggest some variability in the specific nanocluster composition from the second gradient. Some HPLC-isolated species resulted in a larger 625 nm absorbance peak and for other instances the 709 nm absorbance peak had a higher intensity, with the emission peak only slightly blue shifting (*Fig 4.1*).

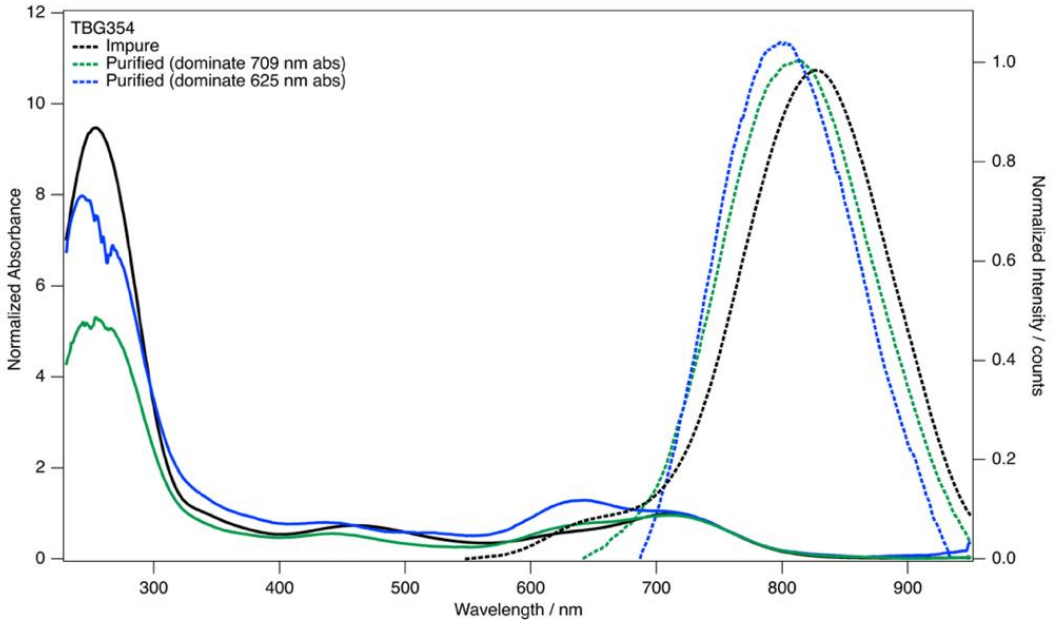

Figure 4.1. *TBG354 purified absorbance and emission spectra compared to impure Ag_N-DNA spectra. The black line what the nanocluster spectra looks like before purification. The green spectra represent a pure species with a dominate 709 nm abs peak and the blue is the spectra for a pure species with a dominate 625 nm peak.*

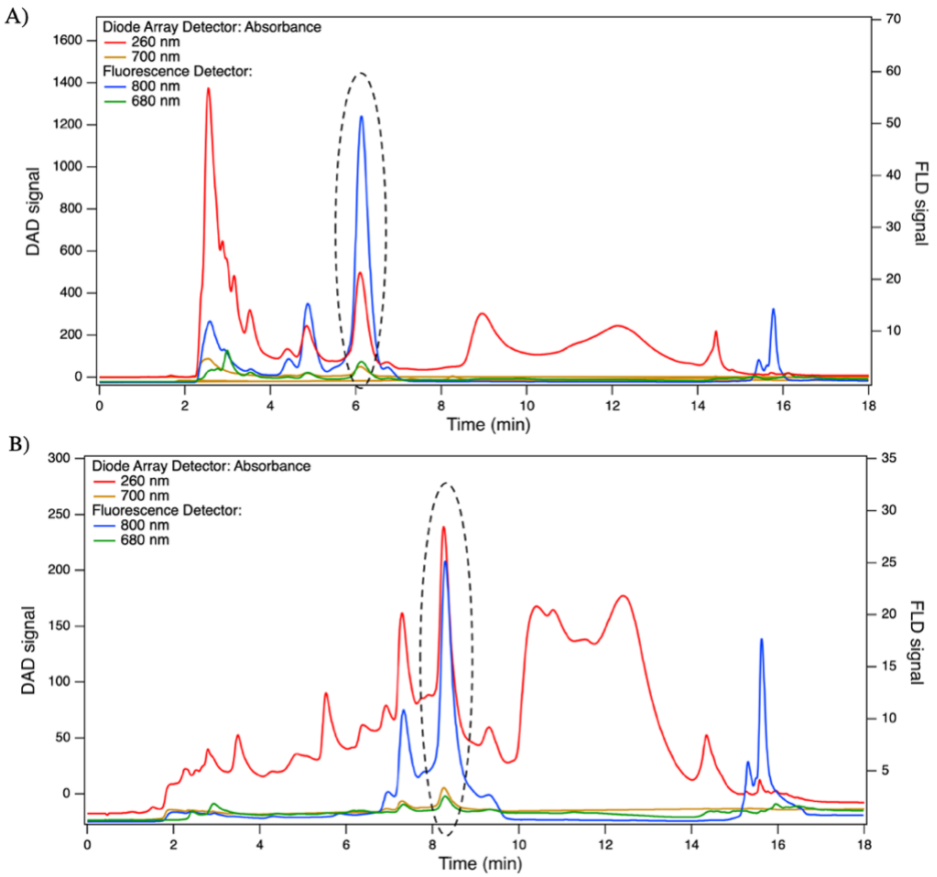

Figure 4.2. *TBG354 HPLC chromatograms for an 85-75% gradient and B) a 90-75% gradient. Target eluents marked with the dashed ovals.*

This nanocluster species is not suitable for bioimaging as it loses its luminescence in physiological conditions, but its ESI-MS results help us better understand the properties of NIR-emissive Ag_N-DNAs. ESI-MS shows that TBG354 has a total of 19 silvers, with 15 cationic silvers and 6 neutral silvers (N_0= 6) (*Fig. 4.3B*). ESI-MS was performed multiple times on different HPLC-purified fractions and always yielded the same total number of silvers. *Figure 4.3A* shows the best-resolved mass spectrum, for the sample with highest concentration of the target nanocluster. $z=5^-$ and $z=4^-$ are the two prominent charge states, with isotopic distributions results for $z=5^-$ seen *Figure 4.3B*. The effective valence electron number 6 supports that this Ag_N-DNA is rod-shaped and could share similar properties to nanoclusters that emit at red wavelengths.[19] When this Ag_N-DNA was tested in a 0.9% saline solution at a 1:1 ratio (roughly matching physiological conditions), the emission

was quenched almost instantly indicating that TBG354's photophysical properties are not stable in saline conditions (*Fig. 4.4*). The nanocluster is stable in a smaller concentration of 25 µM NaCl although an additional species forms around 650 nm.

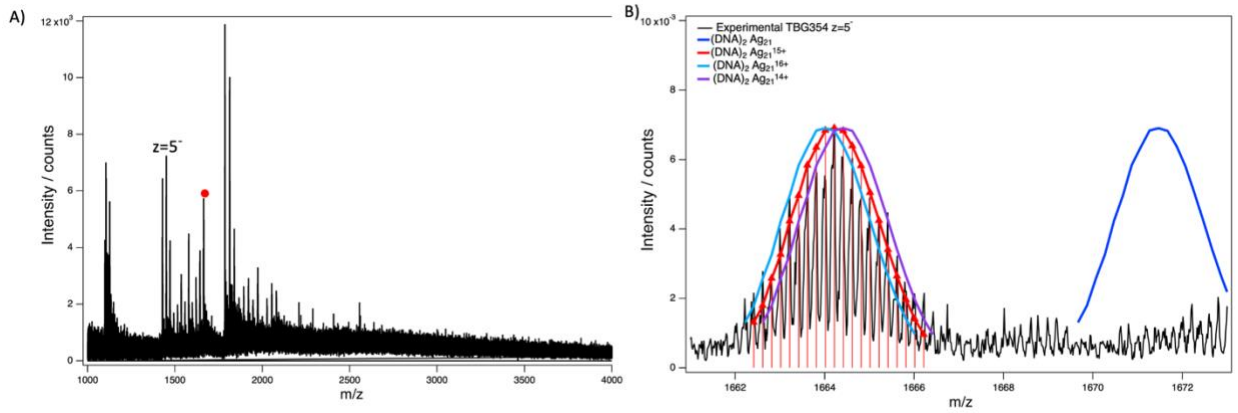

Figure 4.3. *A) TBG354 mass spectrum collected by negative ion mode ESI-MS. Fits were performed for the peak associated with the largest silver atom number (identified with the red dot). B) z=5⁻ results for the best isotopic distribution at 21 silvers with a charge of 15 ⁺.*

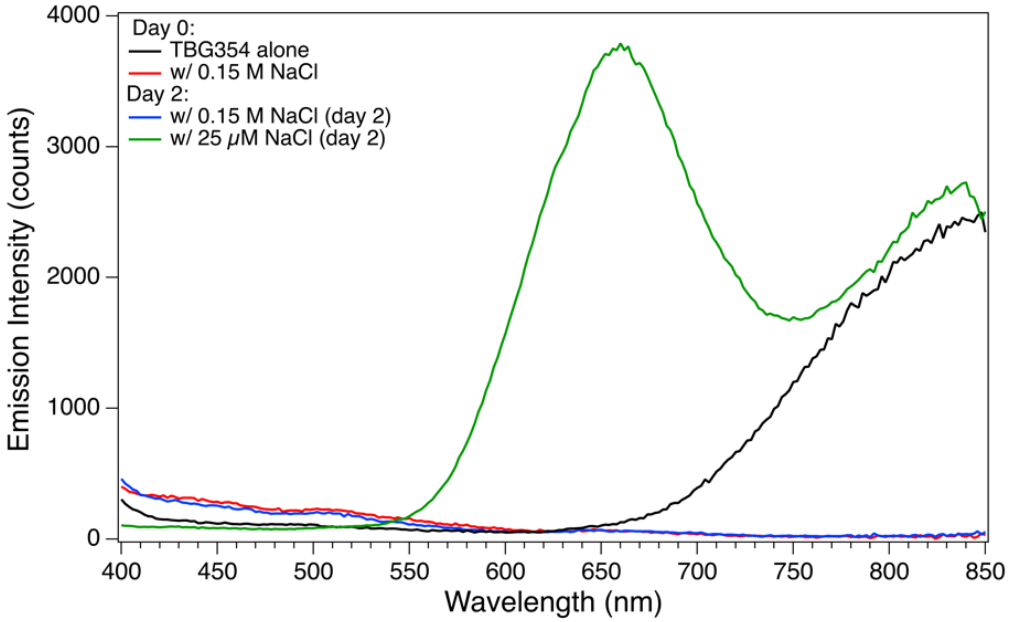

Figure 4.4. *TBG354 emission drops dramatically after mixing with 0.15M (0.9%) NaCl on day 0 and 2 but with a smaller concentration of 25 µM NaCl, the nanocluster is stable.*

TBG66: new species formation leads to a pure NIR-emissive nanocluster

Ag_N-DNA species TBG66, with emission at the start of the NIR I window, showed to have fairly consistent HPLC chromatograms and its purified absorbance spectrum was further confirmed using circular dichroism (CD) measurements. This Ag_N-DNA species, stabilized by the DNA oligomer sequence 5-ACCGCCGGA-3', was synthesized with final concentrations of 20 µM DNA, 10 mM NH_4OAc, 300 µM $AgNO_3$, and 150 µM $NaBH_4$, resulting in emission peaked at 784 nm. As discussed earlier in Chapter 3, this nanocluster was discovered by heating reduced solutions of DNA and silver salt; this nanocluster does not form without increased temperatures during the nanocluster formation process. The optimal HPLC gradient was found to be 89-75%, with the target product eluting between 2 and 4 minutes (*Fig.4.5*). This nanocluster has three defined absorbance peaks in its pure form at 580 nm, 475 nm, and 407 nm (*Fig. 4.6*). This is unusual for a pure Ag_N-DNA, which typically has only one or two absorbance peaks. Although a greater concentration of TBG66 is needed to achieve high quality CD spectra for this emitter, the CD spectral features align with the purified absorbance peaks, including negative CD signatures at 580 nm and 407 nm and a positive peak at 475 nm (*Fig. 4.7*). The CD spectral features at UV wavelengths are due to the chirality of the DNA ligand and its interactions with Ag^+ cations.

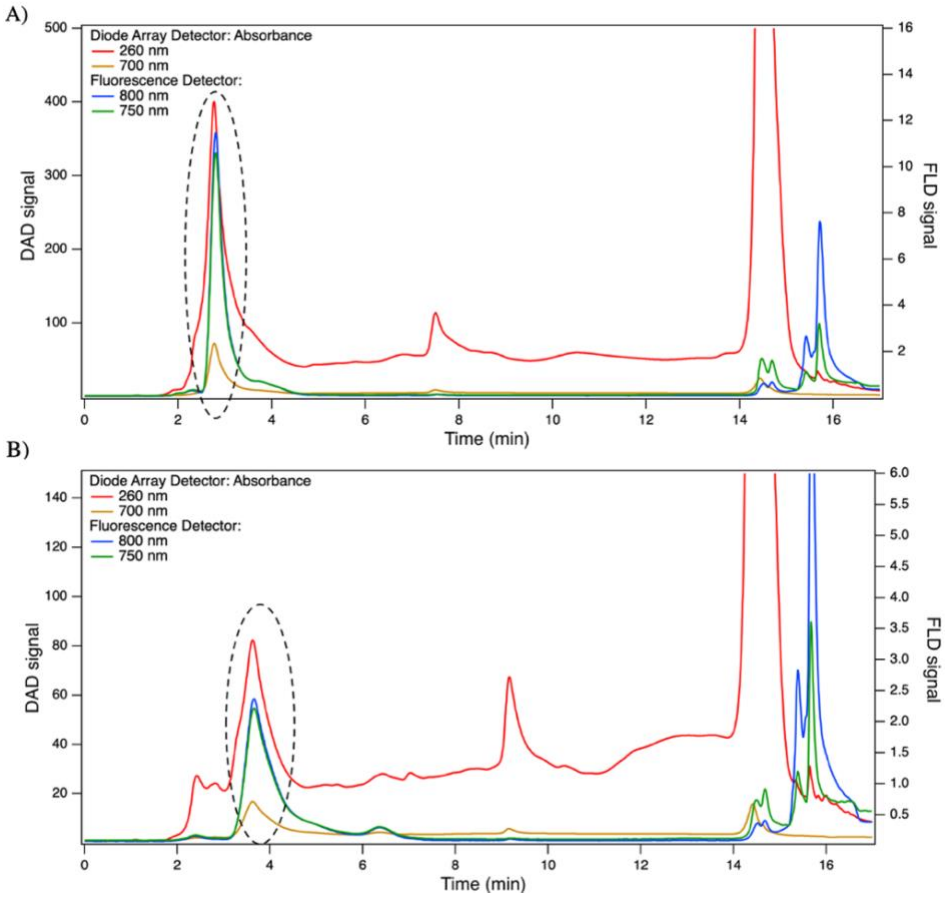

Figure 4.5. *TBG66 HPLC chromatograms. The aliquots collected (dashed ovals) show target eluents. Chromatograms are shown for A) an 88-75% gradient and B) an 89-75% gradient. Chromatograms were found to be consistent for different gradient conditions.*

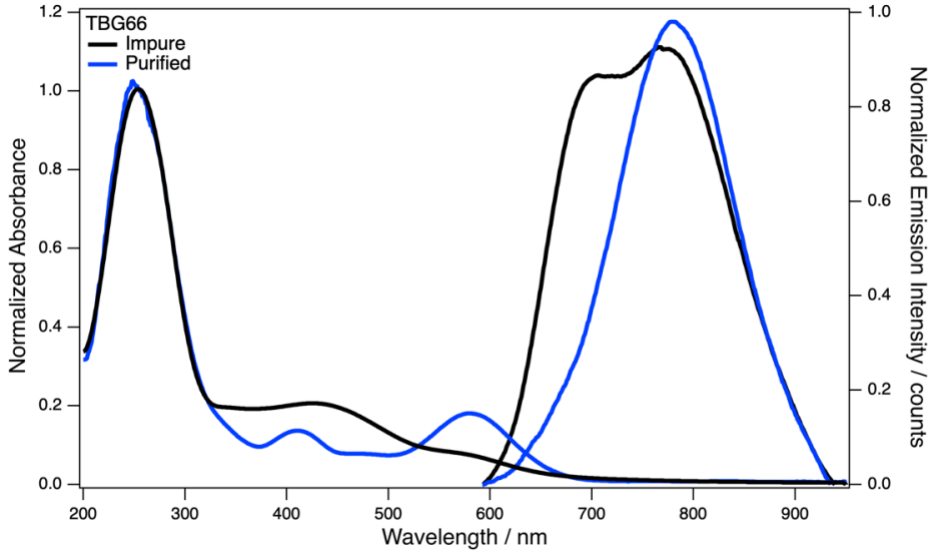

Figure 4.6. *Comparison of absorbance and emission spectra of TBG66 before (black) and after (blue) HPLC purification.*

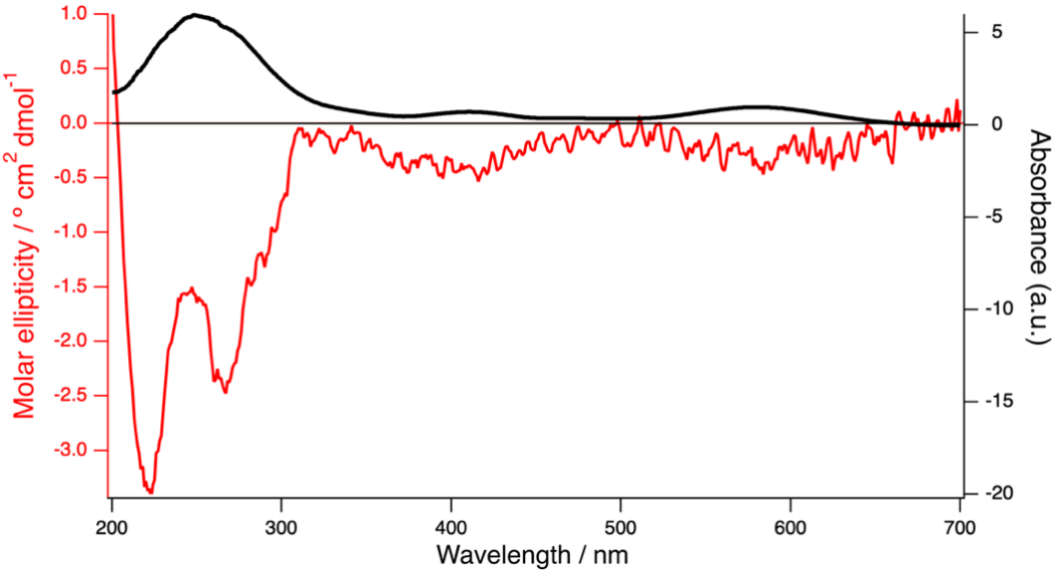

Figure 4.7. *Circular Dichroism (CD, red) and absorbance (black) spectra of TBG66 measured by Rweetuparna Guha.*

This Ag_N-DNA species, similar to TBG354, was also predicted to have a rod-like cluster shape and was found to be unstable in physiological solutions. Mass spectra of TBG66 indicated a total of 19 silver, with an effective valence electron number of $N_0 = 6$ and a charge of +13 (*Fig. 4.8B*) This suggests that TBG66 has rod-like cluster shape. Fragmentation in the mass spectrometer was observed, as the most intense peak in the mass spectrum corresponded to 17 total silvers with $N_0 = 6$ (*Fig. 4.9C*), while the larger nanocluster species had 19 total silvers. Because N_0 does not change, it is possible that the ESI-MS process strips off some weakly bound silver cations.[17] Lastly, this nanocluster's emission was quenched when exposed to a 0.9% saline solution at a 1:1 ratio indicating this Ag_N-DNA lost its photophysical properties in physiological conditions (*Fig. 4.9*).

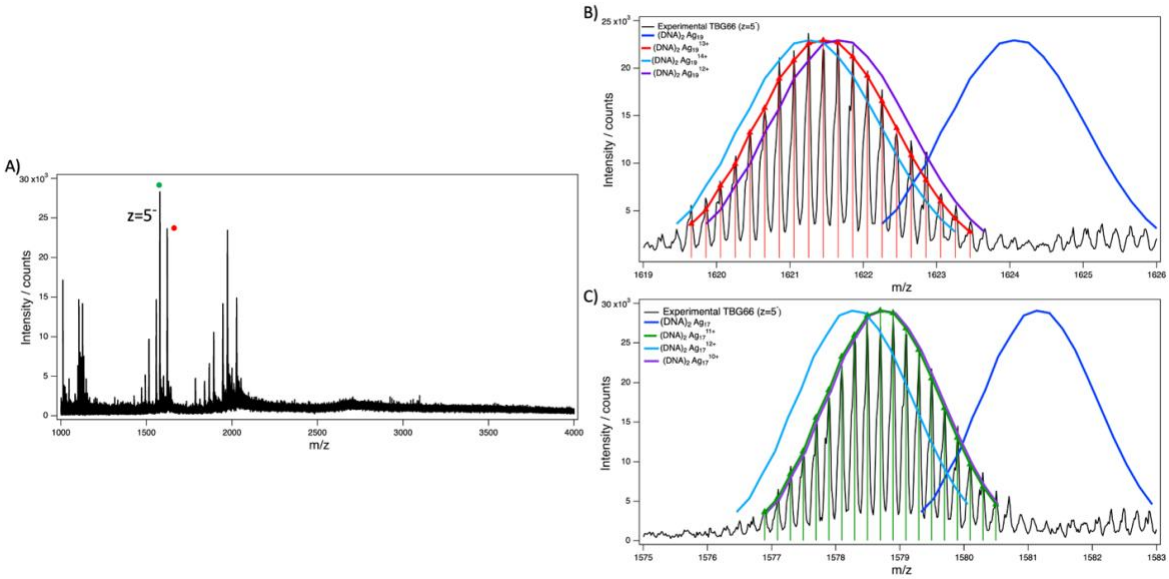

Figure 4.8. *A) Mass spectra of TBG66. Fits were performed for the peak associated with highest silver atom content (indicated with red dot) and the most intense peak (indicated green dot). B) and C) shows various calculated isotopic mass distribution, with the best isotopic distributions at B) 19 silvers with a charge of +13, and C) 17 silvers with a charge of +11.*

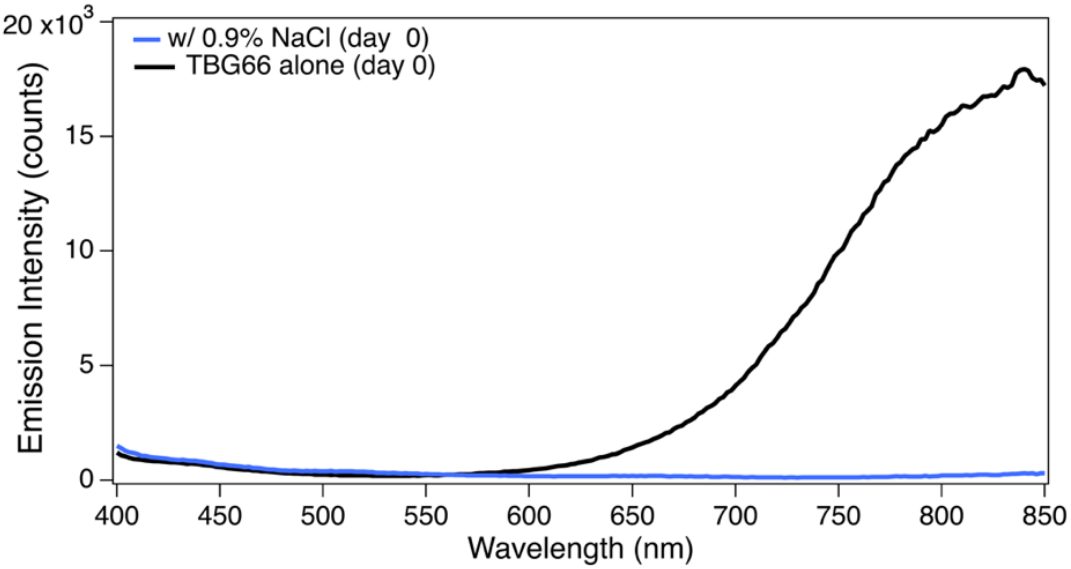

Figure 4.9. *TBG66 emission drops dramatically after mixing with 0.15 M (0.9%) NaCl on day 0, indicating that this nanocluster is not stable in saline solutions.*

These two NIR- emissive Ag_N-DNAs, TBG354 and TBG66, share many similar characteristics that help us better understand the photophysical properties of NIR-emissive nanoclusters. The chemical yield of both NIR I Ag_N-DNAs are optimized with post-reduction at room temperature.

Additionally, both Ag_N-DNAs have N_0= 6 neutral silver atoms, which supports rod-like cluster structure. Lastly, these Ag_N-DNAs have three absorbance peaks in their purified form. Although these are only two examples of NIR-emissive Ag_N-DNAs, their similar properties suggest that these commonalities may be shared by many other NIR-emissive nanoclusters.

TBG203: evidence for chloride ligands

Although this Ag_N-DNA, TBG203, does not emit in the NIR I window, it is unique for its stability in saline. With a DNA template sequence of 5-CACCCCGAGC-3', this nanocluster in its unpurified form has an emission peak at 719 nm, with absorbance peaks at 535 nm and 420 nm. When we first purified TBG203, we measured an emission peak around 700 nm and a dominate absorbance peak at 478 nm with a second peak at 580 nm (*Fig. 4.10*). Unsure of the cause to the blue shift in the emission peak, we decided to test the nanocluster's stability in NaCl. TBG203 was mixed in a 1:1 ratio with 0.9% NaCl and then purified by HPLC. Mixing with NaCl further blue-shifted the emission peak from the original 719 nm, forming a new species at 685 nm with an increased intensity and also resulted in the loss of the 580 nm absorbance peak. *Figure 4.11* compares the chromatograms of A) the 700 nm TBG203 species and B) the 685 nm TBG203 species formed after mixing with NaCl. The optimal HPLC gradients did not vary much without NaCl; the gradient was found to be 80-65% without NaCl, and when mixed with NaCl, the ideal gradient was 85-65%. Similarly, both gradients caused the target species to elute around 2-3 minutes.

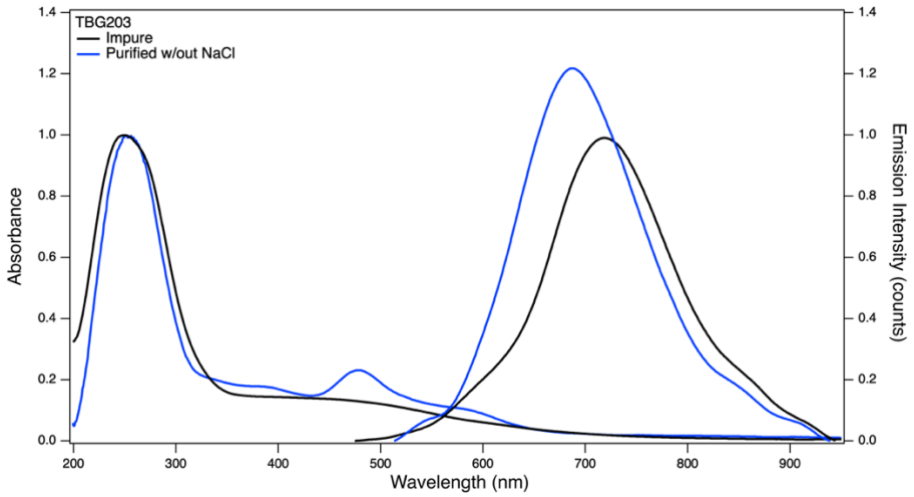

Figure 4.10. *Purified TBG203 absorbance and emission spectra compared to impure Ag$_N$-DNA spectra.*

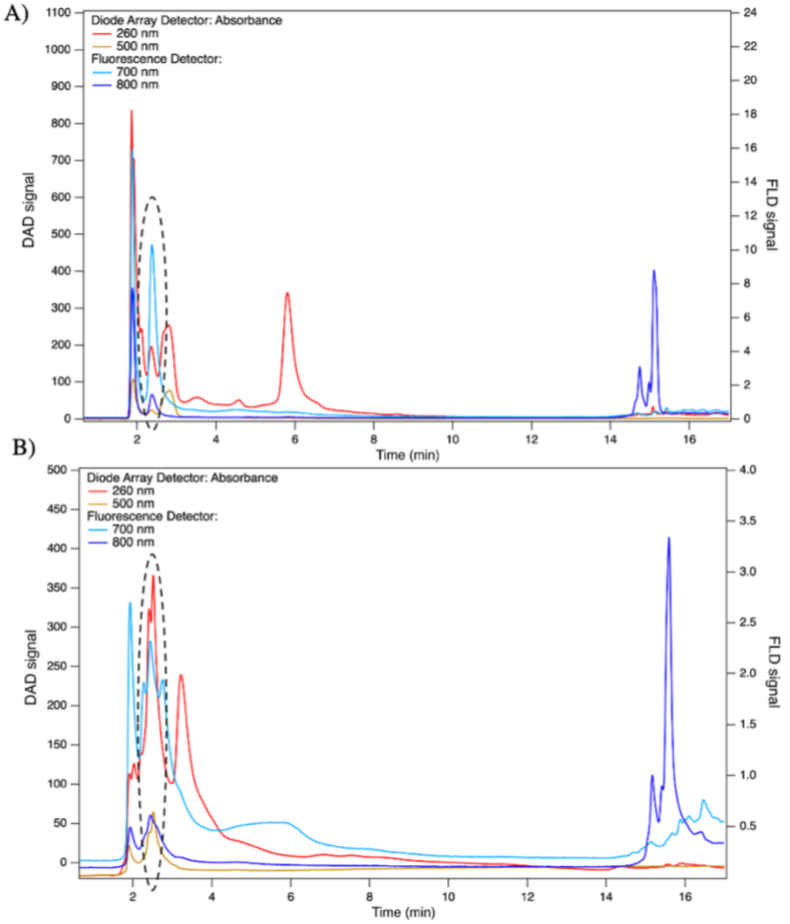

Figure 4.11. *HPLC chromatogram of TBG203. The aliquots collected (dashed ovals) show target eluents. Chromatograms are shown for A) an 80-65% gradient for TBG203 700 nm species and B) an 85-75% gradient for TBG203 mixed with NaCl 685 nm species. Chromatograms were found to be similar for different gradient conditions.*

Recent findings in the Copp lab suggest that chlorine ligands can sometimes be present on Ag_N-DNAs, and TBG203 provides additional evidence for this. Preliminary results of ESI-MS for the 700 nm species (without addition of NaCl) indicate the presence of 2 chlorine atoms along with 22 total silvers and 6 neutral silvers (*Fig. 4.12*). Further purification and MS measurements are required to confirm the potential of chlorines because the ESI-MS results for the 685 nm species is unclear at this time. Despite the fact that we add no chlorine-containing compounds during nanocluster synthesis, the discovery of chlorines in the core of this nanocluster agrees with evidence of other Ag_N-DNAs with chlorines (*publication in preparation*). Additionally, when the 685 nm species was purified, the intensity decreased compared to the intensity prior to purification. This drop in emission intensity could result from washing out extra non-bonded chlorines from the solution during purification that aided in intensifying the nanocluster's emission.

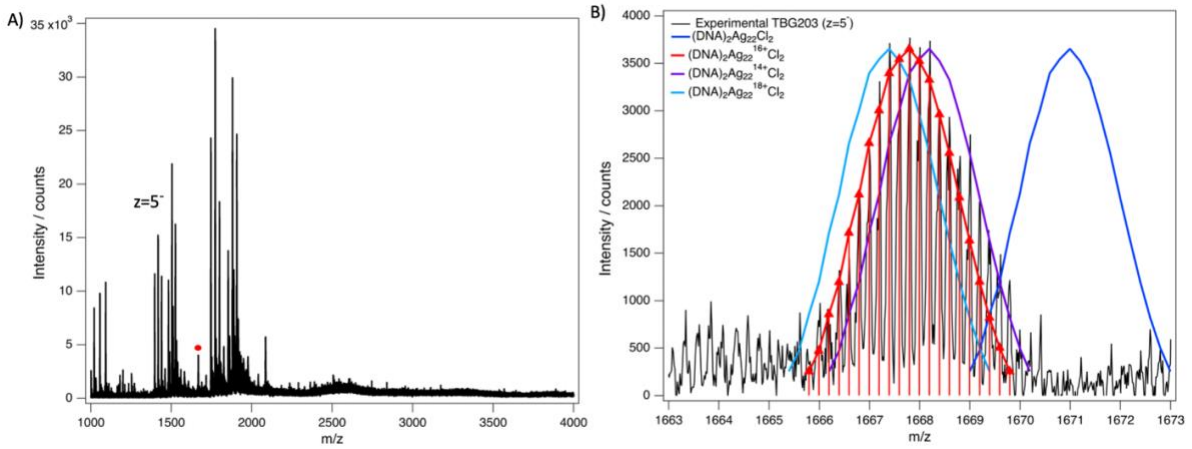

Figure 4.12. *A) Mass spectrum of TBG203 containing the 700 nm species. Fits were performed for the peak associated with the largest silver atom number (identified with the red dot). B) shows initial fittings comparing different charges with the best isotopic distribution at 22 silvers with a charge of +16 and 2 chlorine atoms.*

Since the addition of NaCl to TBG203 produced a promising increase in the emission intensity but also resulted in a blue shift of the emission peak, it was predicted that the mixed NaCl concentration was too high. Therefore, we performed NaCl sweeps from final concentration of 25

µM up to 1000µM of NaCl to determine the optimal concentration that would generate an increase in the emission intensity without causing a blue shift. A 750 µM concentration of NaCl in a 3:1 of ratio (Ag_N-DNA:NaCl) was found to be optimal (*Fig. 4.13*). The purification for TBG203 with 750 µM of NaCl initially appears to have a varied chromatogram where the aliquot is collected around 10 minutes, but a pure sample has not yet been achieved.

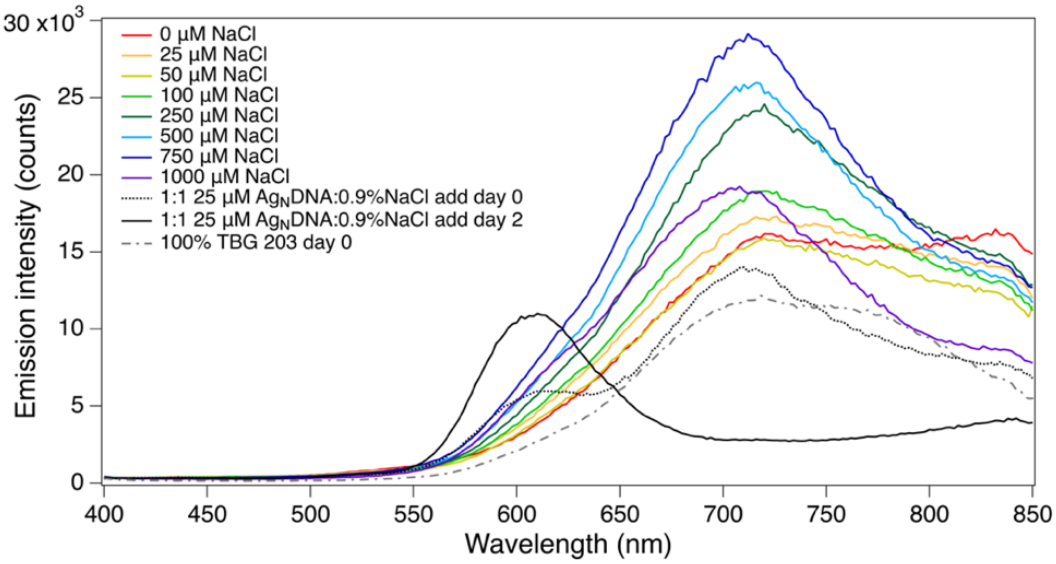

Figure 4.13. *NaCl concentration sweeps for TBG203 where 750 µM yields the highest intensity without blue shifting the emission.*

In summary, this chapter highlighted three successfully purified Ag_N-DNAs, their chemical properties, photophysical properties, and their stability in physiologically relevant NaCl concentrations. The commonalities among these NIR-emissive Ag_N-DNAs provide insights into the structure-property relationships of Ag_N-DNAs. Lastly, this chapter shows that certain Ag_N-DNAs may be well-suited for *in vivo* studies.

CHAPTER 5: Preliminary *in vivo* tests and future directions

Enabled by our growing development of NIR-emissive Ag_N-DNAs, we tested one saline stable nanocluster in mouse model. This preliminary study aimed to test for the first time how Ag_N-DNA fluorescence persists *in vivo*, how long the nanoclusters remain stable and/or circulate in the blood, and what their toxicity is. This step towards *in vivo* experiments is crucial in developing an understanding of how the Ag_N-DNAs behave not only in saline conditions, but in the presence of all the cells, proteins, and sugars found in blood.

We chose GG322 for mouse studies since this nanocluster is the brightest and most stable in saline conditions and has a resolved crystal structure.[6] The study consisted of three mice. Saline was injected into the tail of a control mouse. A low dose of GG322 was injected into the vein in the tail of a second mouse, and a high dose was injected into the lower abdominal region of a third mouse (*Figure 5.1*). Images were taken using a filter cube centered at 570 nm excitation and 737 nm emission (Cy 5). The fluorescence from the Ag_N-DNA was evident from images taken with both 1 second and 3 minute exposure times. Preliminary results indicated no histological difference in the spleen and liver between the control and experimental mice, potentially indicating that the Ag_N-DNA are not toxic to the mice. Although these results and experiments require further trials and histological analyses, these results motivate the exciting potential of Ag_N-DNAs as promising fluorophores. Our work supports that NIR-emissive Ag_N-DNAs have the potential to be functional biolabels that are stable in physiological conditions, fluorescent in the NIR I region, and can greatly improve deep tissue biomedical imaging.

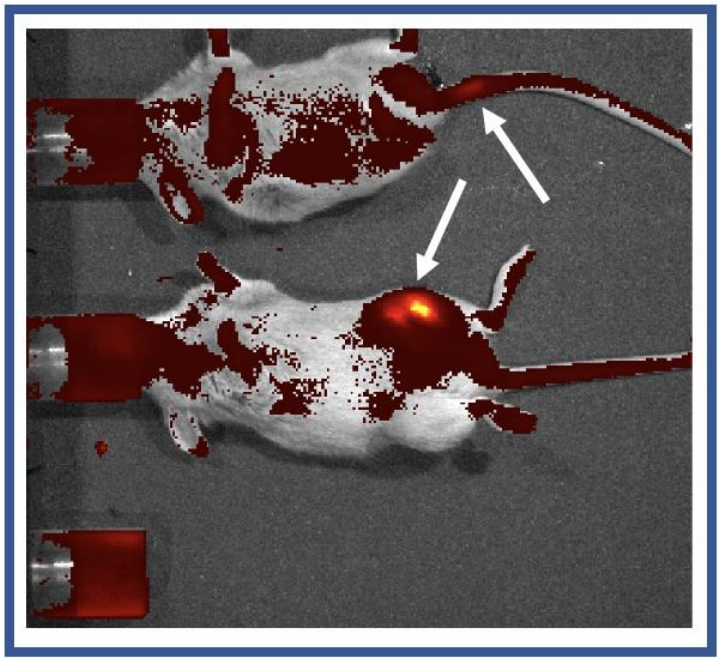

Figure 5.1. *Fluorescence images of NIR-emissive Ag_N-DNA GG322 after injection into mice and imaged after several hours. Arrows indicate injection sites. The top mouse had a low dose injected into the tail, and the bottom mouse had a high dose injected into the abdomen.*

CONCLUSION

In an effort to advance current bioimaging techniques, this thesis is focused on discovering and optimizing implementable NIR-emissive Ag_N-DNA fluorophores for subsequent optical microscopy applications. As evident from experiences with COVID-19 and other life-altering illnesses, humans are very fragile, and a person's health can quickly be affected by unforeseen sicknesses and circumstances. Therefore, advancements in biomedical technology must evolve as quickly as diseases do. The drive to improve bioimaging techniques could play a promising role in protecting many aspects of human health.

This thesis was successful in advancing the understanding of NIR-emissive Ag_N-DNAs, focusing on their chemical and photophysical properties. The new discovery that tuning post-reduction temperature conditions can increase the chemical yield of the known NIR-emissive nanoclusters, help form new NIR-emissive Ag_N-DNAs species that evolve from red/far red Ag_N-DNAs, and decrease the overall time it takes a nanocluster to achieve maximum brightness will greatly benefit future NIR-emissive nanocluster exploration. This important finding saves time, increases emission intensity up to 50-fold, and suggests that there are many more Ag_N-DNAs capable of forming NIR-emissive species than were previously known. Secondly, the three successfully purified NIR-emissive Ag_N-DNAs, although not all stable in physiological conditions, aided in developing a foundational understanding of the compositional properties of these nanoclusters, including their expected number of DNA strands and neutral silver atoms, and how these characteristics relate to their photophysical properties. This basis is crucial because the more evidence collected on the compositional interactions of these nanoclusters, the easier it will be to predict possible NIR-emissive candidates and develop crystal structures. This work also points to groundbreaking new evidence of chlorine ligands in some nanoclusters that has previously never

been reported. Additionally, we discovered that although polyamines do not improve stability of Ag_N-DNAs in physiological conditions, some of these nanoclusters can survive on their own in saline conditions, leading to encouraging *in vivo* mice studies. Preliminary results of NIR-emissive Ag_N-DNAs injected into mice show nanocluster fluorescence remains unchanged *in vivo*, with no overt signs of toxicity to mice. This is a promising indication that NIR-emissive Ag_N-DNAs make great candidates as fluorophores for optical microscopy with the potential of safe biomedical applications.

Future studies focus on the continuation of discovering and characterizing Ag_N-DNAs that emit in the NIR I window, with a keen focus on nanoclusters that are stable in physiological conditions. With an increased knowledge of the chemical and photophysical properties of saline-stable NIR-emissive Ag_N-DNAs, researchers will be better equipped to determine which nanoclusters are most applicable for in-depth *in vivo* mouse studies and toxicity screenings. Lastly, ongoing exploration of chloride ligands in Ag_N-DNAs have the potential to change our understanding of the chemical properties and crystal structure of Ag_N-DNAs and to create new classes of these emitters that are especially well-suited for biomedical applications.

REFRENCES

(1) Hong, G.; Antaris, A. L.; Dai, H. Near-Infrared Fluorophores for Biomedical Imaging. *Nat Biomed Eng* **2017**, *1* (1), 0010. https://doi.org/10.1038/s41551-016-0010.

(2) Pansare, V. J.; Hejazi, S.; Faenza, W. J.; Prud'homme, R. K. Review of Long-Wavelength Optical and NIR Imaging Materials: Contrast Agents, Fluorophores, and Multifunctional Nano Carriers. *Chemistry of Materials* **2012**, *24* (5), 812–827. https://doi.org/10.1021/cm2028367.

(3) Lavis, L. D.; Raines, R. T. Bright Ideas for Chemical Biology. *ACS Chem Biol* **2008**, *3* (3), 142–155. https://doi.org/10.1021/cb700248m.

(4) Yang, J.; Yang, F.; Zhang, C.; He, X.; Jin, R. Metal Nanoclusters as Biomaterials for Bioapplications: Atomic Precision as the Next Goal. *ACS Materials Letters*. American Chemical Society July 4, 2022, pp 1279–1296. https://doi.org/10.1021/acsmaterialslett.2c00237.

(5) Chen, Y.; Phipps, M. L.; Werner, J. H.; Chakraborty, S.; Martinez, J. S. DNA Templated Metal Nanoclusters: From Emergent Properties to Unique Applications. *Acc Chem Res* **2018**, *51* (11), 2756–2763. https://doi.org/10.1021/acs.accounts.8b00366.

(6) Gonzàlez-Rosell, A.; Cerretani, C.; Mastracco, P.; Vosch, T.; Copp, S. M. Structure and Luminescence of DNA-Templated Silver Clusters. *Nanoscale Adv* **2021**. https://doi.org/10.1039/D0NA01005G.

(7) Copp, S. M.; Gonzàlez-Rosell, A. Large-Scale Investigation of the Effects of Nucleobase Sequence on Fluorescence Excitation and Stokes Shifts of DNA-Stabilized Silver Clusters. *Nanoscale* **2021**. https://doi.org/10.1039/D0NR08300C.

(8) Gonzàlez-Rosell, A.; Guha, R.; Cerretani, C.; Rück, V.; Liisberg, M. B.; Katz, B. B.; Vosch, T.; Copp, S. M. DNA Stabilizes Eight-Electron Superatom Silver Nanoclusters with Broadband Downconversion and Microsecond-Lived Luminescence. *J Phys Chem Lett* **2022**, 8305–8311. https://doi.org/10.1021/acs.jpclett.2c02207.

(9) ThermoFisher Scientific. *The Molecular Probes ® Handbook - Introduction to Fluorescence Techniques.*, 11th ed.; 2010.

(10) Chalfie, M.; Tu, Y.; Euskirchen, G.; Ward, W. W.; Prasher, D. C. Green Fluorescent Protein as a Marker for Gene Expression. *Science (1979)* **1994**, *263* (5148), 802–805. https://doi.org/10.1126/science.8303295.

(11) Vale, R. D.; Funatsu, T.; Piercet+, D. W.; Romberg, L.; Harada, Y.; Yanagida, T. *Direct Observation of Single Kinesin Molecules Moving along Microtubules*; 1996.

(12) Swasey, S. M.; Leal, L. E.; Lopez-Acevedo, O.; Pavlovich, J.; Gwinn, E. G. Silver (I) as DNA Glue: Ag+-Mediated Guanine Pairing Revealed by Removing Watson-Crick Constraints. *Sci Rep* **2015**, *5* (1), 10163. https://doi.org/10.1038/srep10163.

(13) Mastracco, P.; Gonzàlez-Rosell, A.; Evans, J.; Bogdanov, P.; Copp, S. M. Chemistry-Informed Machine Learning Enables Discovery of DNA-Stabilized Silver Nanoclusters with Near-Infrared Fluorescence. *ACS Nano* **2022**. https://doi.org/10.1021/acsnano.2c05390.

(14) Häkkinen, H. Atomic and Electronic Structure of Gold Clusters: Understanding Flakes, Cages and Superatoms from Simple Concepts. *Chem Soc Rev* **2008**, *37* (9), 1847–1859. https://doi.org/10.1039/b717686b.

(15) Ponnuswamy, N.; Bastings, M. M. C.; Nathwani, B.; Ryu, J. H.; Chou, L. Y. T.; Vinther, M.; Li, W. A.; Anastassacos, F. M.; Mooney, D. J.; Shih, W. M. Oligolysine-Based Coating Protects DNA Nanostructures from Low-Salt Denaturation and Nuclease Degradation. *Nat Commun* **2017**, *8*. https://doi.org/10.1038/ncomms15654.

(16) Petty, J. T.; Zheng, J.; Hud, N. v.; Dickson, R. M. DNA-Templated Ag Nanocluster Formation. *J Am Chem Soc* **2004**, *126* (16), 5207–5212. https://doi.org/10.1021/ja031931o.

(17) Copp, S. M.; Gorovits, A.; Swasey, S. M.; Gudibandi, S.; Bogdanov, P.; Gwinn, E. G. Fluorescence Color by Data-Driven Design of Genomic Silver Clusters. *ACS Nano* **2018**, *12* (8), 8240–8247. https://doi.org/10.1021/acsnano.8b03404.

(18) Schultz, D.; Gardner, K.; Oemrawsingh, S. S. R.; Markešević, N.; Olsson, K.; Debord, M.; Bouwmeester, D.; Gwinn, E. Evidence for Rod-Shaped DNA-Stabilized Silver Nanocluster Emitters. *Advanced Materials* **2013**, *25* (20), 2797–2803. https://doi.org/10.1002/adma.201204624.

(19) Copp, S. M.; Schultz, D.; Swasey, S.; Pavlovich, J.; Debord, M.; Chiu, A.; Olsson, K.; Gwinn, E. Magic Numbers in DNA-Stabilized Fluorescent Silver Clusters Lead to Magic Colors. *J Phys Chem Lett* **2014**, *5* (6), 959–963. https://doi.org/10.1021/jz500146q.